Published in final edited form as:

Pflugers Arch. 2017 February ; 469(2): 195–212. doi:10.1007/s00424-016-1911-9.

FHF2 isoforms differentially regulate Nav1.6 mediated resurgent sodium currents in dorsal root ganglion neurons

Cindy Barbosa[1,2], **Yucheng Xiao**[1,2], **Andrew J. Johnson**[1,2], **Wenrui Xie**[3], **Judith A. Strong**[3], **Jun-Ming Zhang**[3], and **Theodore R. Cummins**[1,2,4,*]

[1]Dept. of Pharmacology and Toxicology, Indiana Univ., Indianapolis, IN

[2]Stark Neurosciences Research Institute, Indiana University School of Medicine, Indianapolis, IN

[3]Dept. of Anesthesiology, Univ. of Cincinnati, Cincinnati, OH

[4]Dept. of Biology, Indiana University – Purdue University Indianapolis

Abstract

Nav1.6 and Nav1.6 mediated resurgent currents have been implicated in several pain pathologies. However, our knowledge of how fast resurgent currents are modulated in neurons is limited. Our study explored the potential regulation of Nav1.6 mediated resurgent currents by isoforms of Fibroblast growth Factor Homologous factor 2 (FHF2) in an effort to address the gap in our knowledge. FHF2 isoforms colocalize with Nav1.6 in peripheral sensory neurons. Cell line studies suggest that these proteins differentially regulate inactivation. In particular, FHF2A mediates long-term inactivation, a mechanism proposed to compete with the open-channel blocker mechanism that mediates resurgent currents. On the other hand, FHF2B lacks the ability to mediate long-term inactivation and may delay inactivation favoring open-channel block. Based on these observations, we hypothesized that FHF2A limits resurgent currents, whereas, FHF2B enhances resurgent currents. Overall our results suggest that FHF2A negatively regulates fast resurgent current by enhancing long-term inactivation and delaying recovery. In contrast FHF2B positively regulated resurgent current and did not alter long-term inactivation. Chimeric constructs of FHF2A and Navβ4 (likely the endogenous open channel blocker in sensory neurons) exhibited differential effects on resurgent currents suggesting that specific regions within FHF2A and Navβ4 have important regulatory functions. Our data also indicate FHFAs and FHF2B isoform expression are differentially regulated in a radicular pain model and that associated neuronal hyperexcitability is substantially attenuated by a FHFA peptide. As such, these findings suggest that FHF2A and FHF2B regulate resurgent current in sensory neurons and may contribute to hyperexcitability associated with some pain pathologies.

*Corresponding Author: Theodore R. Cummins, Department of Biology, 723 W. Michigan St., SL306, Indianapolis, IN 46202-2266, Phone: 317-278-9343, trcummin@iupui.edu.

AUTHOR'S CONTRIBUTIONS

CB participated in design of study, carried out sub-cloning, mutagenesis, surgical procedures, immunocytochemical assays and patch-clamp experiments with corresponding analysis, and was involved in draft and revision of the manuscript. AJ contributed in the design of LID experiments, surgical procedures, and immunocytochemical assays with corresponding analysis and was involved in the revision of the manuscript. YX carried out patch-clamp experiments with corresponding analysis and was involved in revision of the manuscript. WZ was involved in experimental design, surgical procedures and behavioral assays. JAS was involved in experimental design and writing of the revised manuscript. JMZ was involved with experimental design, interpretation of the data and revision of the manuscript. TRC was involved in design of the study, interpretation of data and was involved in draft and revision of manuscript.

Keywords

Resurgent Na+ current; Resurgent current; Fibroblast growth factor homologous factor; FHF; dorsal root ganglia neurons

INTRODUCTION

Voltage gated sodium channels (VGSC) selectively mediate the inward flow of sodium ions generating the rapid upstroke of the action potential (26, 41). As such alteration of sodium channel activity can be an underlying mechanism in neurological pathologies (31) including but not limited to pain (8, 10, 12, 61). Painful sensations can commonly arise from increased firing of peripheral sensory neurons in Dorsal Root Ganglia (DRG) and Trigeminal Ganglia (49). Adult DRG neurons normally express a variety of VGSC isoforms that can be distinguished based on their sensitivity to tetrodotoxin (TTX) inhibition resulting in two classes: TTX-Sensitive (TTXS: Nav1.1, 1.6, Nav1.7) and TTX-Resistant (TTXR: Nav1.8 and Nav1.9) channels (4, 13–15, 25). Some of these VGSC isoforms can generate an unusual current known as resurgent current (6, 22, 28, 44, 55). Resurgent currents are generated when VGSCs open (upon membrane depolarization) and an open channel blocker out-competes the intrinsic mechanism of inactivation (fast inactivation) and blocks the channels in the open conformation (1, 21, 34). This open channel block mechanism temporarily terminates further sodium influx because as the membrane repolarizes the blocker unbinds and sodium influx resurges (46). Thus, resurgent currents generate a depolarizing drive during membrane repolarization that may enable the generation of another action potential (47). In this manner, resurgent currents contribute to increased neuronal activity.

Two types of resurgent currents have been identified in DRG neurons based on their kinetics: fast and slow. Under normal conditions, Nav1.6 predominantly mediates fast resurgent currents (6), whereas Nav1.8 mainly mediates slow resurgent currents (55). In this study we investigate how fast resurgent currents are modulated in DRG neurons. There is a breadth of evidence that implicates fast resurgent currents in increased neuronal activity and pain pathologies such as: radicular pain (71), oxaliplatin acute painful neuropathy (53), ATX-II induced pain (29), and Paroxysmal Extreme Pain Disorder (28, 56). Interestingly, recent studies using animal models of inflammatory, neuropathic and chemotherapeutic induced pain suggest Nav1.6 has an important role in mediating painful sensations (9, 38, 52, 53, 68, 70). Together these findings suggest targeting Nav1.6 mediated activity, such as resurgent currents, may provide novel strategies for pain therapeutics. However, our understanding of how fast resurgent currents are modulated in DRG neurons is fairly limited. Sodium channel auxiliary subunits are potential candidates for resurgent current modulation. For example, we recently reported that sodium channel beta 4 subunit (Navβ4) is a major determinant of resurgent currents in DRG neurons (3). Our results were consistent with Central Nervous System (CNS) studies, which proposed the C-terminal sequence of this subunit acts as an open channel blocker (2, 21, 39). In particular, a region of 20 amino acids within the cytoplasmic C-terminal region (known as the β4 peptide) is predicted to be key for Navβ4 positive regulation of fast resurgent currents (57, 75). Inclusion of the β4

peptide in cell lines and neurons that do not endogenously generate resurgent currents evokes them (42, 51). Similar effects are observed in DRG neurons, where inclusion of the β4 peptide or expression of the full length Navβ4 protein evokes and enhances resurgent currents (64). In contrast, overexpression of a mutant form of Navβ4 in which key residues within the β4 peptide region were neutralized reduced resurgent current generation further confirming the importance of this region for resurgent current generation.

Fibroblast Growth Factor Homologous Factors (FHF1–4 also known as FGF11–14) are another family of auxiliary proteins that recent studies suggest regulate resurgent currents in CNS neurons (57, 75). Contrary to their homologue counterpart, FHFs are not secreted and function independent of fibroblast growth factor receptors (42, 51). Thus, FHFs are intracellular signaling proteins that have multiple interacting partners including microtubules (64), kinases (62), scaffolding proteins (50, 51), nuclear factors (30), calcium channels (74) and VGSCs (19, 77). FHF interaction with VGSC can alter the biophysical properties of activation, inactivation and current density (19, 43). Adult DRG neurons can express a variety of FHF isoforms including FHF1, FHF2 and FHF4 (27, 35, 48, 63, 77). Each FHF gene can result in different isoforms through alternative splicing and promoter usage resulting in distinct N-terminal sequences (40). “A” and “B” isoforms have conserved core domains that enable them to bind to the C-terminus of sodium channels (18, 36, 58, 60).

FHF “A” isoforms have two distinct features: 1) a long N-terminal sequence and 2) a bipartite nuclear localization signal (NLS), which may be active or inactive depending on the cell background (54). FHFAs unique N-terminus expresses a peptide sequence (which is highly conserved between all FHFAs) that may interact with VGSC channels and induce long-term inactivation (16). This long-term inactivation particle competes with the intrinsic mechanism of inactivation (fast inactivation). Open channel block, which mediates resurgent currents, also competes with fast inactivation (34). Based on these observations, Goldfarb et al. (2012) proposed that long-term inactivation might compete with open-channel block (20). In a Nav1.5 cell line addition of long-term inactivation peptide reduced β4-peptide mediated resurgent currents supporting the possibility that these particles compete with each other (57). In contrast, FHF “B” isoforms do not mediate long-term inactivation but may alter voltage dependence and kinetics of inactivation in ways that likely favor open channel block (19). For example FHF4B in Purkinje neurons increased resurgent currents by slowing the rate of inactivation and shifting the voltage dependence of inactivation to positive potentials increasing the probability of binding for the endogenous open channel blocker (75). It is important to note that not all FHF isoforms are reported to have the same effect with all VGSC isoforms. For Nav1.6, heterologous co-expression of FHF2 and FHF4 isoforms consistently caused a shift in the voltage dependence of inactivation to positive potentials, whereas, differential effects were observed in current density depending on VGSC isoform and cell background. In ND7/23 cells FHF2 isoforms exhibited differential effects in response to trains of stimulation. FHF2A caused accumulation of inactivation at all frequencies due slowing recovery from inactivation, whereas, FHF2B protected the channel from inactivation at high frequencies with no change in recovery (48, 63). In this study, we investigate the role of FHF2 isoforms (also known as FGF13) in regulating fast resurgent currents because they have been shown to co-localize with Nav1.6 (the main carrier of fast resurgent current) in DRG neurons. Therefore we hypothesized that FHF2A inhibits fast

resurgent currents in sensory neurons through long-term inactivation. In contrast, FHF2B lacks the ability to mediate long-term inactivation and may alter inactivation favoring open channel block similar. Therefore, we hypothesized that FHF2B increase resurgent currents by delaying inactivation.

Our results show that FHF2A negatively regulates resurgent currents and enhances long-term inactivation, whereas, FHF2B positively regulates resurgent currents and does not alter long-term inactivation. Data obtained from chimeric constructs of FHF2A and Navβ4 provided insight into the importance of FHF2A's long-term inactivation particle and the Navβ4 open channel blocker sequence for the direction (positive versus negative) of resurgent current modulation. In neurons harvested from animals with localized inflammation of the DRG, we observed reduced FHFAs' expression whereas FHF2B's expression was enhanced. Our findings suggest that this differential modulation of FHF2A and FHF2B could contribute to enhanced resurgent currents and result in sensory neuron hyperexcitability. Interestingly, neuron hyperexcitability associated with localized inflammation of the DRG was substantially reduced by FHFA peptides that induce long-term inactivation. Overall our data indicate that FHFs are important regulators of VGSC activity in sensory neurons and suggest that alterations in FHF2A and FHF2B expression likely contribute to changes in nociception and pain.

METHODS

cDNA constructs

These studies used cDNA constructs of sodium channel auxiliary subunits, FHF2A, FHF2B and chimeric constructs of FHF2A and Navβ4. All constructs were tagged at the C-terminus with photostable monomeric Turquoise2 (pmTurquoise2) to verify expression. To generate the FHF2A and FHF2B tagged constructs, the coding sequence corresponding to mouse FHF2A (NP_034330.2) and human FHF2B (NP_378668.1) were synthesized and purchased from Genscript (Piscataway, NJ). Mouse FHF2A protein is 99.56% identical to human FHF2A (NP_004105.1) and is predicted to be 100% identical to rat FHF2A (NC_005120.4). Human FHF2B protein is 99.48% identical to mouse (NP_001277344.1) and rat FHF2B (NP_445880.1). The FHF2A sequence was cut from a pUC57 vector and inserted into pmTurquoise2-N1 vector with HindIII/KpnI restriction enzymes. The FHF2B sequence was cut from pcDNA3.1 (+) vector and inserted into pmTurquoise2-N1 vector with HindIII/BamHI restriction enzymes. The sequences were moved in-frame by site directed mutagenesis (Quikchange XL II Site Directed Mutagenesis kit, Agilent Technologies).

The chimeric constructs of FHF2A and Navβ4 were designed in-house by replacing the long-term inactivation particle sequence (AAAIASSLIRQKRQARAREREK, 20 amino acids (16)) with the Navβ4 open-channel blocker sequence (KKLITFILKKTREKKKECLV, 20 amino acids (33)) to generate the F2A(β4) construct. Conversely, the open channel sequence in rat Navβ4 (NP_001008880.1) was replaced with the long-term inactivation particle of FHF2A to generate the (β4)F2A construct. The full chimeric sequences were synthetically made and purchased from Genscript (Piscataway, NJ). The F2A(β4) and (β4)F2A sequences were cut from the pUC57 vector and sub-cloned into pmTurquoise-N1 with NheI/XhoI

restriction enzymes. To move the sequences in frame with the fluorescent protein the stop codon was mutated to a glycine residue using site-directed mutagenesis.

To study Nav1.6 in isolation from endogenous TTXS channels we used a Nav1.6 TTXR construct previously described in (44). Briefly, the sequence corresponding to human Nav1.6 protein (NP_055006.1) was codon-optimized and purchased from Genscript (Piscataway, NJ). The sequence was then sub-cloned into pcDNA3.1 (+) with KpnI/XbaI restriction enzymes. The Nav1.6 sequence was then modified with site directed mutagenesis to confer high resistance to TTX by converting tyrosine residue 371 to serine as previously described (24, 32). The resulting construct was named Nav1.6r. Additionally, we knocked down endogenous TTXR Nav1.8 channels with a small hairpin RNA (shRNA) plasmid to aid in the isolation of Nav1.6r currents. The Nav1.8 shRNA-IRES-dsRED plasmid encoded for Nav1.8 shRNA sequence (targeting sequence, GATGAGGTCGCTGCTAAG, (37) and an internal ribosome entry site for the translation of fluorescent protein marker dsRed (IRES-dsRED) as previously described (3, 28).

Cell culture

DRG neurons were obtained from adult male Sprague Dawley rats. Rats were euthanized by CO_2 exposure and secondary decapitation. The spinal column was then removed and DRG were harvested from the lumbar to cervical region. The nerve processes were cut from the excised ganglia. Ganglia were then digested in Dulbecco' modified Eagle's Medium (DMEM, Fisher Scientific) containing collagenase (1.25 mg/mL) and neutral protease (0.78 mg/mL) for 45 minutes at 37 °C. Subsequently, the digested ganglia were centrifuged at 1000rpm for five minutes. Digestion media was aspirated and replaced with 10% Fetal Bovine Serum (FBS, Hyclone) DMEM (Invitrogen) and ganglia were mechanically triturated with sequentially smaller glass pipettes. Triturated ganglia were spun again at 700 rpm for five minutes. Media was aspirated and replaced with fresh 10% FBS DMEM media. Aliquots of cell suspension (~100uL) were loaded unto glass coverslips coated with poly-D-lysine and laminin. After 10 minutes, cells settled and 500uL of 10% FBS DMEM was added to each well. For electrophysiological experiments with transfected neurons, the 10% FBS DMEM media was supplemented with mitotic inhibitors, 5-fluoro-2-deoxyuridine (50uM, Sigma Aldrich) and uridine (150uM, Sigma Aldrich), to prevent overgrowth of the supporting cells. Dissociated cultures were maintained at 37°C in a humidified 95% air and 5% CO_2 incubator. Media was changed every two days.

For Localized Inflammation of the DRG (LID) experiments, L4 and L5 ipsilateral DRG were excised from sham operated rats and inflammation induced rats at post-operative day 5. The above dissociation protocol and culture was followed with the exception of the digestion time, which was decreased to 28 minutes. Indiana University School of Medicine Institutional Animal Care and Use Committee approved the animal protocols described above.

Surgical procedure for localized inflammation of the DRG

Localized inflammation of the DRG was used as a model of radicular pain as previously discussed in (76) and described in (66). Adult male Sprague Dawley rats under isoflurane

anesthesia were used for these procedures. After deep anesthesia was verified, an initial incision on the back near the spinal column was made from L3–S1 to expose and visualize the superficial area of the spine. Then, a second deeper incision was made on one side of the animal approximately 1mm from the center of the spine from L4 to S1. Paraspinal muscles near L4/L5 were carefully teased apart until intervertebral foramen could be visualized using the transverse processes, ilium and dorsal/ventral ramus as guides. Aliquots of 10uL containing zymosan diluted in incomplete Freud Adjuvant (2mg/mL) were injected above L4 and L5 DRG, through a needle inserted close to the DRG through the intervertebral foramen. The needle was bent in a 90 degree angle ~2 mm from the tip for easier access and was left for two minutes after injection to prevent leakage. After injection, the area was sutured by layers. Sham operated animals were used as a control; the above procedure was followed with the exception of zymosan injection. Indiana University School of Medicine and University of Cincinnati Institutional Animal Care and Use Committees approved the surgical procedure described.

Behavioral measurements

Mechanical sensitivity was tested by applying a series of von Frey filaments to the heel region of the paws on animals with L5 localized inflammation, using the up-and-down method (5). A cutoff value of 15 grams was assigned to animals that did not respond to the highest filament strength used. A fine wisp of cotton was stroked mediolaterally across the plantar surface of the hindpaws to score the presence or absence of a brisk withdrawal response to a normally innocuous mechanical stimulus (light touch-evoked tactile allodynia). This stimulus does not evoke a response in normal animals. Cold sensitivity (cold allodynia) was scored as withdrawal responses to a drop of acetone applied to the ventral surface of the hind paw. When observed, responses to acetone or light brush strokes consisted of several rapid flicks of the paw and/or licking and shaking of the paw; walking movements were not scored as positive responses. Hypersensitivity to thermal (heat) stimuli was not examined because we have previously observed that this is little affected by LID (72). The tester was blinded as to the sham or LID status of the animals. All data presented are from the ipsilateral side; in this model the contralateral side shows little or no hypersensitivity in any of the tests used (data not shown). Behavioral time course data were analyzed using two-way repeated measures ANOVA with Bonferroni post hoc test to determine on which days experimental groups differed. The experimental protocol was approved by the Institutional Animal Care and Use Committee of the University of Cincinnati.

Immunocytochemistry

To study the expression pattern of FHF2A and FHF2B after inflammation, L4 and L5 ipsilateral DRG ganglia were harvested and cultured from sham operated and inflammation induced animals at post-operative day 5. DRG neurons were fixed after 24 hours in culture, permeabilized, blocked and treated with antibodies in the following manner: Cells were fixed with 4% paraformaldehyde (0.1 M phosphate buffer, pH 7.4) for 20 min at room temperature, washed with phosphate buffered saline (PBS), permeabilized in 1% Triton X-100 in PBS for 20 min at room temperature, washed with PBS, blocked for 2 h (10% normal goat serum, 0.1% Triton X-100 in PBS) at room temperature, washed with PBS, incubated in primary antibodies diluted in blocking solution overnight at 4°C, washed with

PBS and incubated with secondary antibody in blocking solution for 2 h at room temperature. Primary antibodies used were Anti-Pan-FHF-A (1:200, Clone N235/22, UC Davis/NIH NeuroMab Facility) and monoclonal Anti-FGF13/FHF2.B (1:200, Clone N225A/10, UC Davis/NIH NeuroMab Facility). Secondary antibody used was Alexa Fluor® 488 Goat Anti-Mouse IgG (Molecular Probes, Life Technologies) at 1:750 concentration. Coverslips were mounted unto microscope slides with Prolong Gold Antifade (Molecular Probes). DRG neurons were imaged using Axio Observer Z1 Widefield Microscope with a 20X objective (ZEISS Microscopy). Images were analyzed using NIS Elements Advance Research (Nikon®) software by defining each cell as a region of interest and quantifying the mean intensity signal for FHF2A and FHF2B. The mean intensity signal was compared between sham and LID groups using Student's t-test. Quantification experiments were carried out independently at least five times; more than 1000 cells were counted for each condition.

Recombinant Expression in DRG neurons

DRG neurons were transiently co-transfected with Nav1.6r, tagged auxiliary subunit and Nav1.8 shRNA-IRES-dsRED using the Helios Gene Gun (Bio-Rad Laboratories) 36–48 hours after dissociation in 2:1:1 ratio respectively. As a negative control, pmTurquoise 2 (tag only) was co-transfected instead of the auxiliary subunits. For peptide studies, only Nav1.6r and Nav1.8 shRNA-IRES-dsRED were co-transfected. Expression of the Nav1.6r construct with Nav1.8 shRNA allowed us to study the modulation of Nav1.6r by auxiliary subunits in isolation from endogenous channels as previously described (3, 28). Although endogenous TTXR Nav1.8 channels run down in culture (17, 28), by using the Nav1.8 shRNA-IRES-dsRED plasmid we further decreased Nav1.8 to minimize contamination. TTXR Nav1.9 currents are not observed under our recoding parameters as previously reported (7, 11). Endogenous TTXS channels were blocked with 500nM.

Electrophysiology and Data Analysis

General Setup—Whole-cell patch-clamp recordings obtained with a HEKA EPC-10USB amplifier. Data were acquired on a Windows-based Intel 2 Core computer using the Patchmaster program (version 2X65; HEKA Elektronik). Fire polished glass electrodes (0.7–1.1 MΩ) were fabricated using a P-97 puller (Sutter), and tips were coated with dental wax to minimize capacitive artifacts and enhance series resistance compensation. The offset potential was zeroed prior to seal formation. Capacitive transients were canceled using computer-controlled circuitry; C-fast for pipette-capacitance correction and C-slow for cell-capacitance compensation. Voltage errors were minimized by series resistance compensation >75%. Membrane currents were sampled at 20 KHz and filtered online at 10 KHz. Leak currents were linearly cancelled by P/-5 subtraction (pulse/number). Whole-cell patch-clamp recordings in voltage clamp mode were obtained 2–3.5 days after transfection at room temperature (~22 °C). Cells examined were selected based on fluorescence of Turquoise (corresponding to auxiliary subunit) and dsRed (corresponding to Nav1.8 shRNA) signal. For peptide studies, the dsRed signal only was used as selection criteria since no auxiliary subunits were co-transfected. Cells with residual Nav1.8 current greater than 3% of the peak current of Nav1.6r were excluded. Nav1.8 contamination was determined by examining the voltage-dependence of steady-state fast inactivation as described previously (3). Whole-cell

voltage clamp recordings were started five minutes after the whole-cell configuration was obtained.

For current-clamp recordings, DRG neurons were allowed to settle at their resting potential. Spontaneous activity was defined as firing observed during 2 minutes with zero current injection. DRG neurons were examined for evoked activity with a series of 2 s current injection from 100 pA to 500 pA in 100 pA increments. For evoked activity, the maximum number of action potentials elicited from each cell was determined as the maximum action potentials elicited from current injections from 0 to 500 pA. Electrophysiology data were analyzed using the software programs Origin (version 8, OriginLab), Fitmaster (v2X65, HEKA Electronik), Excel (Microsoft) and final graphs were made in Prism (version 6, GraphPad).

Recording solutions—The electrode solution consisted of 140 mM CsF, 10 mM NaCl, 1.1 mM EGTA, and 10 mM HEPES (adjusted to pH 7.3 with CsOH). The extracellular bathing solution contained 130 mM NaCl, 30 mM TEA chloride, 1mM MgCl2, 3 mM KCl, 1mM CaCl2, 0.05 mM CdCl2, 10 mM HEPES and 10 mM D-glucose (adjusted pH 7.3 with NaOH). For current-clamp recordings, the pipette solution contained 140 mM KCl, 0.5 mM EGTA, 5mM HEPES and 3 mM Mg-ATP (adjusted pH 7.3 with KOH). The extracellular solution contained 140 mM NaCl, 3 mM KCl, 2 mM MgCl2, 2 mM CaCl2 and 10 mM HEPES (adjusted pH 7.3 with NaOH). Recording solutions were adjusted using D-glucose to maintain physiological osmolarity values.

Peptide Experiments—To study the effects of FHF2A`s long-term inactivation particle, we used a peptide corresponding to amino acids residues 2–21 as reported in (16). The peptide, FHFA, was modified with an N-terminal acetyl group and C-terminal hydroxyl group yielding the following sequence: Ac-AAAIASSLIRQKRQARAREK-OH (purchased from Biopeptides Co). The FHFA peptide was added to the electrode solution at a 1mM concentration. Control groups included either having no peptide added to the intracellular solution or adding an inactive mutant FHFA-5Q peptide (Ac-AAAIASSLIRQQQQAQEQEQ-OH from Biopeptides Co) to the electrode solution at a 1mM concentration.

Steady-State Activation—Current-voltage (I/V) relationships were determined by steps of 50 ms, from −100 to + 80mV, in 5 mV increments. The voltage-dependence of activation (m_∞) was determined from sodium currents elicited with I/V protocol from voltages of −100 mV to 0 mV. Conductance (G) values were calculated at each test potential (V_m) using the reversal potential (V_r) with following equation, $G=\frac{I}{(V_m - V_r)}$. Data was then normalized to the peak conductance, plotted as a function of voltage and fitted using single-phase Boltzmann distribution equation, $\frac{G}{G_{max}}=\left(\frac{1}{1+e^{\left(V_m - V_{1/2}\right)/k}}\right)$. The midpoint points ($V_{1/2}$) and slope factor (k) were obtained for each cell.

Steady-State Inactivation—Steady-state fast inactivation (h_∞) was assayed with 500 ms pre-pulses from −130 to 5 mV (in 5 mV increments) followed by a 20 ms test pulse to −20 mV to assess channel availability. Current Peak currents at each pre-pulse were normalized to the overall peak current. Data of normalized currents as a function of voltage was fitted with the single phase Boltzmann distribution, $\frac{I}{I_{max}} = \left(\frac{1}{1+e^{\left(V_m - V_{1/2}\right)/k}} \right)$, from which the midpoint points ($V_{1/2}$) of steady-state fast inactivation and slope factor (k) were obtained for each cell. Additionally, current densities were estimated for each individual recording by dividing the peak transient currents obtained from h_∞ by the membrane capacitance.

Recovery from Inactivation—Recovery from Inactivation was assayed with a two-pulse protocol that depolarized the membrane to −20 mV for 20 ms from holding potential (−100mV). The time between the pulses was increased by an additive 2^n factor, where n=sweep number. At each time point the peak current measured in the second pulse (I_2) was normalized to the peak current measured in the first pulse (I_1), yielding fraction available. Fraction available $\left(\frac{I_2}{I_1}\right)$ was plotted as a function of time (t) and fitted to a double exponential equation, $\frac{I_2}{I_1} = A_0 + A_{fast} e^{-t/\tau fast} + A_{slow} e^{-t/\tau slow}$, from which we obtained the recovery time constants for the fast (τfast) and slow component (τslow) and compared between groups.

Accumulation of long-term inactivation—Cells were assayed with a four-pulse protocol, as previously described (16), to measure long-term inactivation. Each pulse depolarized the membrane to −20 mV for 16ms from a holding potential of −90mV with −90mV 40 ms interpulse recovery phases between each depolarization pulse. Peak current measured at each pulse was normalized to overall peak current to yield percentage of sodium channels available. The % of channels available was plotted as a function of depolarization cycle (i.e. pulse number).

Resurgent Current—Cells were assayed with a two-pulse protocol that initially depolarized the membrane to +30 mV for 20 ms from the holding potential (−100mV), followed by repolarizing voltage steps from +15 mV to −80 for 100 ms in −5 mV increments to test for resurgent currents; cells were then returned to their holding potential (−100mV). Resurgent currents display unique characteristics of slow onset and slow decay along with a non-monotonic I/V relationship. Currents that did not meet these criteria were classified as negative for resurgent currents. Based on these criteria, the percentage of DRG that were positive/negative for detectable resurgent current was quantified for each condition. Resurgent current amplitudes were measured after 3.0 ms into the repolarizing pulse to avoid contamination from tail currents. Peak resurgent current amplitude at each test potential was normalized to peak transient current (obtained from the h_∞ protocol) and expressed as a percentage of peak transient current. Normalized resurgent current amplitude was plotted as a function of voltage.

Statistics

Data are presented as mean ± standard error of the mean (SEM). The data were tested for Gaussian distribution fit with D'Agostino & Pearson omnibus normality test. Data that fit Gaussian distribution were compared with parametric test, Student's t-test at a 95% level of confidence (α=0.05). Data that did not fit Gaussian distribution were compared with a non-parametric Mann-Whitney Test with 95% level of confidence (α=0.05). The Chi-square test (X^2 test) was used to compare the frequency distribution of resurgent current positive/negative neurons and repetitive action potential firing between groups at a 95% level of confidence (α=0.05).

RESULTS

Biophysical Properties of Nav1.6r with FHF2A and FHF2B

We first examined if in DRG neurons FHF2A could mediate the characteristic long-term inactivation that has been reported in other cells with FHFAs variants (16, 48). Primary cultured DRG neurons were biolistically co-transfected with Nav1.6r and tagged-FHF2A or tagged-FHF2B. As a negative control, tag only (pmTurquoise2; fluorescent protein) was transfected instead of a FHF subunit. Whole-cell voltage-clamp recordings of isolated Nav1.6r were obtained by pharmacological (addition of 500 nM TTX) and genetic (Nav1.8shRNA; see Methods) inhibition of endogenous DRG sodium currents. Long-term inactivation was measured using a four-pulse protocol consisting of depolarizations to −20mV for 16ms with 40ms interpulses at −90 mV as described by Dover et al, 2010 (16). Representative traces obtained with this long-term inactivation assay are shown in Fig. 1a for each group. Overexpression of FHF2A increased accumulation of Nav1.6r in long-term inactivated states, consistent with previous reports (16, 48). FHF2A progressively decreased Nav1.6r availability with each depolarization cycle relative to control (Fig. 1b, minimum sodium channel availability p p<0.0001: FHF2A 72 ± 3%, n=18; Control 90 ± 2%, n=28), whereas, FHF2B did not (p=0.62, FHF2B 91 ± 2%, n=13).

We also examined how FHF2A and FHF2B alter other biophysical properties of Nav1.6r in DRG neurons since in different cell backgrounds FHFs' interaction with VGSCs have been reported to alter current density, inactivation, activation and recovery as previously discussed (43). Current-voltage (I/V) relationship was determined with a single pulse protocol that ranged from −100 to 80mV for 50ms. Using the I/V protocol we quantified peak current density and activation. Overexpression of FHF2A or FHF2B did not alter peak current density of Nav1.6r relative to control (Table 1, p=0.32 and p=0.37 respectively). FHF2A did shift the voltage dependence of activation to more positive potentials (Fig. 1c, p=0.0063), whereas FHF2B did not, relative to control (Table 1, p=0.50). Steady-state inactivation was assayed by conditioning the cells with a pre-pulse that ranged from −130 to 5mV for 500ms followed by a test pulse to −20mV for 20ms. Consistent with previous reports (48, 59, 60, 63), FHF2A and FHF2B shifted the voltage dependence of inactivation to more depolarized potentials (Fig. 1d, p=0.0013 and p=0.026 respectively). Recovery from inactivation was assayed with a two-pulse step protocol that depolarized the membrane to −20mV for 20ms with increasing time between pulses (recovery phases). Fig. 1e shows that FHF2A slowed recovery from inactivation (Table 1; τfast, p=0.16 and τslow, p=0.012), whereas, FHF2B

enhanced recovery from inactivation relative to control (Table 1; τfast, p<0.0001 τslow, p=0.03). Table 1 shows a summary of recovery, inactivation, activation and current density data.

Differential modulation of fast resurgent currents by FHF2A and FHF2B

We next investigated resurgent current modulation by these FHF2 isoforms. To do so we used a two-pulse protocol that initially depolarized the cell membrane to 30mV for 20ms followed with a series of repolarization pulses from +15 to −80 mV for 100ms. Resurgent current amplitudes were normalized to classic sodium peak current (maximum current obtained from the steady-state inactivation protocol) and expressed as percentage of peak current. Representative traces of resurgent currents are shown in Fig. 2a for each group. Overall FHF2A reduced the fraction of resurgent current positive neurons (X^2 test, p=0.039), whereas FHF2B did not, relative to control (Fig. 2b, p=0.60). FHF2A also reduced resurgent current amplitude relative to control (Fig. 2c Peak Resurgent Current Amplitude p=0.0021: FHF2A 0.371 ± 0.21%, n=18; Control 1.14 ± 0.27%, n=29). FHF2B exhibited the opposite effect, doubling peak resurgent current amplitude relative to control (p=0.0034: FHF2B 2.41 ± 0.22%, n=13).

FHFA peptide replicates long-term inactivation effects and reduced Nav1.6r mediated resurgent currents

FHF2A has two known potential interactions that might contribute to Nav1.6r modulation: 1) binding to the C-terminal of sodium channels and 2) long-term inactivation particle binding (presumably to the inner pore region). We hypothesized that FHF2A's long-term inactivation particle is the main contributor for the observed negative regulation of fast resurgent currents. To explore this possibility, we used a peptide (FHFA peptide) corresponding to amino acid residues 2–21 in FHF2A protein, previously identified as the long-term inactivation particle (16). FHFA peptide (1mM) was added to the internal recording solution as described by Dover et al, 2010. DRG neurons were transfected with Nav1.6r and recombinant currents were isolated as described in the methods section. Voltage clamp recordings were obtained five minutes after dialysis of the internal solution in the presence or absence of the peptide. Using the protocols previously described we examined current density, activation, inactivation, recovery, long-term inactivation and resurgent currents. Representative traces of long-term inactivation test are shown in Fig. 3a–b. Dialysis of the FHFA peptide greatly increased accumulation of Nav1.6r in long-term inactivated states (Fig. 3c, minimum sodium channel availability p<0.0001: +FHFA 29 ± 3%, n=15; −FHFA 84 ± 2%, n=16). Recovery from inactivation was significantly slowed in the +FHFA peptide group relative to the −FHFA peptide group (Fig. 3d and Table 2; τfast, p=0.034 and τslow, p=0.012). Addition of the FHFA peptide did not alter Nav1.6r current density (p=0.054), voltage dependence of activation (p=0.21) or inactivation relative to control (p=0.95). Table 2 shows a summary of current density, activation and inactivation data. We next examined resurgent currents with a two-step protocol as previously described. Representative traces of peak Nav1.6r resurgent currents are shown in Fig. 3e. The +FHFA peptide group exhibited reduced resurgent current amplitudes relative to −FHFA peptide group (Fig. 3f, peak resurgent current p<0.0001: +FHFA Peptide 0.3 ± 0.2, n=15; −FHFA Peptide 1.5 ± 0.4%, n=16). The fraction of resurgent current positive neurons was also

greatly reduced in the +FHFA peptide group (Chi-square test p=0.0032: 20%, n=15) relative to control −FHFA peptide (69%, n= 16). An additional set of experiments was performed to determine if these effects were specific to the FHFA peptide or could be induced by any peptide. Dover et al. showed that substitution of five charged residues in the N-terminus of FHF2A with glutamines eliminates the ability of FHF2A to induce long-term inactivation (16). We synthesized the corresponding FHFA-5Q peptide and added it at 1 mM to the internal recording solution. When neurons recorded with FHFA-5Q peptide (n=14) were compared to neurons recorded with no added peptide (n=7) there was no difference in terms of accumulation in long-term inactivated states (p=0.66), kinetics of recovery from inactivation (p=0.90) and resurgent current amplitude (p=0.74), indicating that FHFA peptide effect is dependent on the specific amino acid sequence.

Modulation of Nav1.6r by chimeric constructs of Navβ4 and FHF2A

The FHF2A long-term inactivation particle is potentially inhibiting fast resurgent currents by out-competing the open-channel blocker Navβ4 (3). Therefore, we investigated if replacing the proposed open-channel blocker sequence in Navβ4 with FHF2A's long-term inactivation sequence would transfer the long-term inactivation activity and reduce resurgent currents in DRG neurons. Conversely, we replaced the long-term inactivation sequence in FHF2A with the open channel blocker in the Navβ4 protein and hypothesized that this construct would increase resurgent current. The sequences were codon optimized and synthetically made (see Methods section). The resulting chimeric constructs were named F2A(β4) for the FHF2A protein containing the Navβ4 open channel sequence and β4(F2A) for the Navβ4 protein containing the FHF2A long-term inactivation sequence (Fig. 4). Both constructs were tagged at the C-terminus with a fluorescent protein, pmTurquoise2, to verify expression. DRG neurons were biolistically transfected with Nav1.6r and a chimeric construct. As a control, tag only was expressed instead of a chimeric subunit. Nav1.6r currents were isolated following inhibition of endogenous sodium currents as previously described. Using the recording protocols previously described we examined the biophysical properties of Nav1.6r with co-expression of β4(F2A) or F2A(β4) and investigated if the chimeric constructs modulated resurgent currents. Representative traces from a long-term inactivation protocol test for each group are shown in Fig. 5a. β4(F2A) slightly increased accumulation of long-term inactivation relative to control (Fig. 5b: minimum sodium channel availability p=0.034: β4(F2A) 84 ± 2%, n=12; Control 89 ± 2%, n=14), whereas, F2A(β4) did not alter accumulation of long-term inactivation (88 ± 2%, n=9). Expression of either chimera, β4(F2A) or F2A(β4) did not alter current density relative to control (Table 3, p=0.82 and p=0.35 respectively). In a similar pattern as seen with FHF2A, F2A(β4) expression shifted the voltage dependence of activation (Fig. 5c, p=0.047) and inactivation (Fig. 5d, p=0.0089) of Nav1.6r to positive potentials relative to control, whereas β4(F2A) did not alter either (Table 3, p=0.36 and p=0.29, respectively). Expression of F2A(β4) enhanced Nav1.6r recovery from steady-state inactivation relative to control (Fig. 5e **Inset**; τfast, p=0.0010 and τslow, p=0.36). β4(F2A) did not slow or enhance Nav1.6r recovery from inactivation relative to control (Fig. 5e and Table 3; τfast, p=0.50 and τslow, p=0.36).

Differential modulation of fast resurgent currents by F2A(β4) and β4(F2A) chimeras

We next examined Nav1.6r mediated resurgent currents with a two-step protocol (Methods section). Resurgent current amplitude was expressed as percentage of peak current. Representative traces of resurgent currents for each condition are shown in Fig.6a. Fig. 6b shows the distribution of resurgent current positive and resurgent current negative neurons for each condition. Overall the percentage of resurgent current positive neurons was not significantly different with expression of β4(F2A) or F2A(β4) relative to control (p=0.30 and p=0.52, respectively). The percentage of resurgent current positive neurons was 33% for β4(F2A), 67% for F2A(β4) and 53% for control. However, F2A(β4) expression increased resurgent current amplitude by three-fold factor relative to control (Fig. 6c peak resurgent current p=0.0023: F2A(β4) 3.1 ± 0.8%, n=9; Control 1.2 ± 0.4%, n=15). In contrast, β4(F2A) exhibited the opposite effect reducing resurgent current amplitude by two-fold factor (β4(F2A) p=0.0076: 0.4 ± 0.2%, n=12).

FHFa in a radicular inflammatory pain model

The results of overexpression of FHF2A and FHF2B, FHFA peptide and chimeric constructs suggest that FHF2A and FHF2B isoforms regulate resurgent currents and may contribute to pain pathologies. We previously reported that resurgent currents are increase in a rat model of radicular pain (71). In this model, localized inflammation of the DRG (LID) causes persistent mechanical hyperalgesia and allodynia that starts as soon as post-operative day 1 (67–69, 71). Therefore, we chose to examine FHF2A and FHF2B expression and the effect of FHFA peptide on neuronal excitability using acutely cultured neurons harvested from rats on day 5 following LID. To examine FHF2A and FHF2B expression, Sprague Dawley Rats were injected with zymosan at a 2mg/mL concentration above the L4 and L5 DRG on one side (see Methods). Sham operated rats that underwent the same procedure with the exception of the injections were used as a control. In order to confirm that the LID but not the sham procedure used evoked pain behaviors on the day the animals were sacrificed for obtaining cultured DRG neurons, behavioral measures of mechanical and cold hypersensitivity were measured at baseline and for 5 days after DRG inflammation or sham surgery. As shown in Supplementary Fig. S1, static and dynamic mechanical allodynia and cold allodynia were significantly elevated in LID animals compared to sham animals, starting as early as POD1 and continuing through POD5. At post-operative day 5, L4/L5 ipsilateral DRG were harvested from LID and Sham operated animals. FHFA and FHF2B levels were examined in primary DRG cultures with immunocytochemistry. One caveat with the FHFA antibody used is that it is not selective to the FHF2A isoform, but rather the antibody used targets the long-term inactivation particle which is highly conserved between all FHFAs. However, in adult DRG neurons, FHF4A is not expressed and FHF1A is downregulated in adulthood (27). FHF1A contains a nuclear localization signal that is functional in DRG neurons and targets the protein to the nucleus (27). In contrast, FHF2A nuclear localization signal is predicted to be inactive since staining is limited to the cell periphery and not detected in the nucleus in adult DRG neurons (48). Therefore, given that our model is an adult DRG neuron we expect that cross-reaction is minimal and likely most of the antibody signal is reflecting FHF2A expression. Representative images of FHFA staining in acutely cultured neurons are shown in Fig. 7a–b. Inflammation of the DRG reduced FHFAs levels relative to Sham control (Fig. 7c, FHF2A Mean Intensity p<0.0001;

LID 13.0 ± 0.3 AU., n=1989, Sham 24.8 ± 0.8 AU, n=1116). In contrast, FHF2B expression was modulated in the opposite direction as FHFAs. Representative images of FHF2B staining are show in Fig.7d–e. FHF2B was upregulated in the LID group relative to Sham control (Fig.7f, FHF2B Mean Intensity $p<0.0001$; LID 29.5 ± 1.6 AU, n=1121, Sham 21.04 ± 0.4 AU, n=1164).

Previously we have shown that local inflammation of the L4/L5 DRG increases spontaneous activity of Aβ neurons and resurgent currents in cultured medium diameter neurons (71). These effects are attenuated by Navβ4 knockdown. Here we asked if LID induced neuronal hyperexcitability could be affected by the FHFA peptide. For this set of experiments we recorded action potential activity from medium diameter neurons harvested from sham and LID treated rats with either 1 mM FHFA peptide or 1 mM FHFA-5Q peptide in the intracellular pipette solution. Neurons from sham animals did not exhibit any spontaneous activity (Fig. 8a–b) with either FHFA-5Q peptide (n=12) or FHFA peptide (n-10) in the pipette solution. By contrast, 3 of 10 neurons from LID treated animals exhibited spontaneous activity with FHFA-5Q peptide in the recording solution (Fig. 8c–d). This is similar to what was observed previously with microelectrode recordings from Aβ fibers in an acutely isolated whole DRG preparation (68, 71). By contrast, no spontaneous activity was observed in neurons when wildtype FHFA peptide was included in the internal recording solution (n=14) and this difference was significant ($p=0.02846$; Chi-square test). Evoked action potential firing was also examined with current injections in the four groups. In both sham and LID treated neurons the wildtype FHFA peptide substantially reduced the number of action potentials compared to the FHFA-5Q peptide (Fig. 8e–h). Significantly more neurons generated multiple action potentials in response to current injections with FHFA-5Q in the pipette than with wildtype FHFA peptide in the pipette ($p=0.00104$; Chi-square test).

DISCUSSION

In this study we show that FHF2A and FHF2B differentially regulate resurgent sodium currents in DRG sensory neurons. The first component of our hypothesis was FHF2A limits the capacity of sensory neurons to generate fast resurgent currents by mediating long-term inactivation. Three main findings support this hypothesis. First, overexpression of FHF2A reduced resurgent current and increased accumulation of channels in inactivated states resulting in delayed channel recovery. Secondly, a peptide derived from FHF2A`s long-term inactivation particle recapitulated the reduction in resurgent current generation and the enhancement of long-term inactivation. The peptide did not modulate the voltage dependence of inactivation and activation as seen with full length FHF2A, suggesting these changes do not account for negative regulation of resurgent current. A mutant peptide (FHFA-5Q) was inactive. Thirdly, the F2A(β4) chimera (in which the long-term inactivation particle was replaced with Navβ4's open channel blocker sequence) did not negatively regulate resurgent currents nor induced long-term inactivation. The chimera produced the opposite effect, an enhancement in resurgent current modulation, suggesting the long-term inactivation particle region is key for FHF2A`s resurgent current modulation.

The second component of our hypothesis was FHF2B increases resurgent currents by delaying inactivation. Our results support this hypothesis. FHF2B increased resurgent current, shifted the voltage dependence of inactivation to positive potentials and enhanced channel recovery. FHF2B's inability to mediate long-term inactivation while shifting inactivation to positive potentials likely increased the accessibility of the putative open channel blocker. The faster recovery observed with overexpression of FHF2B supports this possibility, since recovery when the channel undergoes open-channel block is reported to occur in a shorter time scale than channel recovery from fast inactivation (46). An alternative explanation is that FHF2B displaces the endogenous negative regulation exerted by FHF2A because all FHFs are predicted to bind to a conserved region in C-terminus of VGSCs (18). FHF2A is expressed in neurons of all size classes and is particularly predominant in small diameter neurons (48). The transfected neurons examined in these studies were mostly in the small diameter range. Therefore, it is plausible that displacement of endogenous FHF2A by exogenous FHF2B contributes to some extent to FHF2B's positive regulation of fast resurgent currents.

Based on previous reports, the potential mechanism for FHF2A negative regulation is competition of the long-term inactivation particle with the Navβ4 open-channel blocker (3, 57). The results from FHF2A and Navβ4 chimeras partially support this hypothesis, however the implications of the results obtained with these chimeric proteins is limited by a few caveats. Our assumption was that by replacing the peptide sequence of long-term inactivation with the open-channel blocker and vice-versa the activity would be retained in the resulting chimera. However, the β4(F2A) chimera failed to delay channel recovery and produced a very mild enhancement in accumulation of inactivated states; suggesting that the long-term inactivation particle is not fully functional in the β4(F2A) chimeric construct. Therefore, the reduction in resurgent current observed with the expression of the β4(F2A) chimera is likely due to a dominant negative effect of an inactive Navβ4. In a similar manner, there are two possible contributions to F2A(β4)'s resurgent current enhancement: 1) the Navβ4 open channel blocker sequence is active in the chimera and 2) loss of the long-term inactivation particle allowed other changes in the voltage dependence to favor the endogenous open channel blocker interaction as seen with FHF2B. To further explore the first possibility, we tested the F2A(β4) chimera in a Nav1.5 HEK cell line that does not generate resurgent current unless the β4-peptide is introduced. We found that indeed the F2A(β4) chimera mediated resurgent currents (Supplementary Fig. S2) in the Nav1.5 cell-line. This result favors the possibility that F2A(β4) chimera retains open-channel blocker activity. However, it would be simplistic to assume that the resurgent current enhancement is only due to this activity. It is likely a combined effect of removing a limiting determinant (i.e. long-term inactivation particle), adding an active open channel blocker sequence and the shift in voltage dependence of inactivation contributing to the overall enhancement of resurgent current. Overall, results from β4(F2A) and F2A(β4) chimeras confirmed that regions of the N-terminus of FHF2A and the C-terminus of Navβ4 are important modulators of fast resurgent currents.

FHFs binding to C-terminus of VGSC can cause changes in the biophysical properties of the VGSC (77). Expression of FHF2A, FHF2B or F2A(β4) shifted the voltage dependent inactivation to positive potentials. Since the F2A(β4) chimera lacks the long-term

inactivation particle sequence yet retained the ability to cause shifts in voltage dependence of activation and inactivation, the results suggest that these modulations are mainly an effect of the FHF2 core region binding to the C-terminus of Nav1.6. The shift of inactivation to positive potentials is consistent with previous reports of FHF2 binding to the C-terminus of different sodium channels including Nav1.6 (18, 48, 60, 63). FHF2A and F2A(β4) also shifted activation to positive potentials. Since both F2A(β4) and FHF2A but not FHF2B exerted this effect, it most likely that the N-terminus region that is conserved between F2A(β4) and FHF2A is responsible for this effect.

Interestingly, the chimeras generated for this study might serve as valuable tools for the study of resurgent currents in the future. The (β4)F2A chimera did not significantly alter the voltage dependence of activation or inactivation, recovery from inactivation, or current density. The main effect we detected was a significant reduction in resurgent current. As such, overexpression of this protein in animal models or in-vitro studies might serve as a tool to selectively target attenuation of resurgent currents. On the other hand, the F2A(β4) chimera might serve as a tool to artificially induce fast resurgent currents. The applications for the F2A(β4) might be limited since it alters other channel properties. However, we envisioned that the F2A(β4) chimera might be useful in high-throughput assays to identify compounds that might inhibit resurgent currents.

Overall our data suggest that FHF2A and FHF2B modulate resurgent currents in DRG neurons. The importance of this finding is more evident when we examine how these proteins are regulated in a radicular pain model induced by localized inflammation of the DRG. Our results show that after inflammation FHFAs isoforms are downregulated in acutely isolated neurons, whereas FHF2B was upregulated. We speculate that changes in expression of these isoforms likely contribute to the increased resurgent current generation and hyperexcitability reported in this model (69, 71, 73). The limitation of the antibody specificity precludes us from definitively contributing the effect solely to changes in the FHF2A isoform. However, the high conservation of the long-term inactivation particle between all FHFAs suggest that if other FHFAs were to interact with Nav1.6 they will likely have a similar negative regulation on resurgent currents. Indeed, we find that the FHFA peptide is able to reduce sensory neuron action potential firing and the enhanced spontaneous activity that is observed in acutely isolated neurons following localized inflammation of the DRG. FHFs modulation might also contribute to other pain pathologies. For example, two studies using cDNA arrays reported FHF2 cDNA levels downregulated with no change in FHF1 and FHF4 after peripheral nerve injury (35, 65). Using Expression Atlas (45) from European Bioinformatics Institute and European Molecular Biology Laboratory we found that FHF1 and FHF2 levels are downregulated in DRG neurons after spinal nerve ligation, a chronic pain model. Data corresponded to a RNAseq study by Hammer et al, 2010 (23). Which of the FHF1 and FHF2 isoforms contribute most to these changes is unknown. Our study suggests that FHFs might prove to be novel targets for regulating fast resurgent current in DRG neurons and further study might provide new insight into possible therapeutic strategies for pain.

Supplementary Material

Refer to Web version on PubMed Central for supplementary material.

Acknowledgments

This work was supported by National Institute of Health diversity supplement (NS053422) and Ruth L. Kirschstein National Research Service Award Individual Predoctoral Fellowship (F31NS090837) to CB, NS053422 to TRC, and NS045594 and NS055860 to JMZ.

Abbreviations

DRG	Dorsal root ganglia
INaR	Resurgent sodium current
FHF	Fibroblast growth factor Homologous Factor
CNS	Central Nervous System
PNS	Peripheral Nervous System
shRNA	small hairpin Ribonucleic Acid
cDNA	complementary deoxyribonucleic acid
LTI	long-term inactivation
HEK	Human Embryonic Kidney
VGSC	Voltage Gated Sodium Channel
TTX	Tetrodotoxin
TTXS	Tetrodotoxin-Sensitive
TTXR	Tetrodotoxin-Resistant
LID	Localized Inflammation of the DRG

References

1. Aman TK, Raman IM. Inwardly permeating Na ions generate the voltage dependence of resurgent Na current in cerebellar Purkinje neurons. J Neurosci. 2010; 30:5629–5634. [PubMed: 20410115]
2. Bant JS, Raman IM. Control of transient, resurgent, and persistent current by open-channel block by Na channel beta4 in cultured cerebellar granule neurons. Proc Natl Acad Sci U S A. 2010; 107:12357–12362. [PubMed: 20566860]
3. Barbosa C, Tan ZY, Wang R, Xie W, Strong JA, Patel RR, Vasko MR, Zhang JM, Cummins TR. Navbeta4 regulates fast resurgent sodium currents and excitability in sensory neurons. Mol Pain. 2015; 11:60. [PubMed: 26408173]
4. Caffrey JM, Eng DL, Black JA, Waxman SG, Kocsis JD. Three types of sodium channels in adult rat dorsal root ganglion neurons. Brain Res. 1992; 592:283–297. [PubMed: 1280518]
5. Chaplan SR, Bach FW, Pogrel JW, Chung JM, Yaksh TL. Quantitative assessment of tactile allodynia in the rat paw. J Neurosci Methods. 1994; 53:55–63. [PubMed: 7990513]

6. Cummins TR, Dib-Hajj SD, Herzog RI, Waxman SG. Nav1.6 channels generate resurgent sodium currents in spinal sensory neurons. FEBS Lett. 2005; 579:2166–2170. [PubMed: 15811336]
7. Cummins TR, Renganathan M, Stys PK, Herzog RI, Scarfo K, Horn R, Dib-Hajj SD, Waxman SG. The pentapeptide QYNAD does not block voltage-gated sodium channels. Neurology. 2003; 60:224–229. [PubMed: 12552035]
8. Cummins TR, Sheets PL, Waxman SG. The roles of sodium channels in nociception: Implications for mechanisms of pain. Pain. 2007; 131:243–257. [PubMed: 17766042]
9. Deuis JR, Zimmermann K, Romanovsky AA, Possani LD, Cabot PJ, Lewis RJ, Vetter I. An animal model of oxaliplatin-induced cold allodynia reveals a crucial role for Nav1.6 in peripheral pain pathways. Pain. 2013; 154:1749–1757. [PubMed: 23711479]
10. Dib-Hajj SD, Binshtok AM, Cummins TR, Jarvis MF, Samad T, Zimmermann K. Voltage-gated sodium channels in pain states: role in pathophysiology and targets for treatment. Brain Res Rev. 2009; 60:65–83. [PubMed: 19150627]
11. Dib-Hajj SD, Choi JS, Macala LJ, Tyrrell L, Black JA, Cummins TR, Waxman SG. Transfection of rat or mouse neurons by biolistics or electroporation. Nat Protoc. 2009; 4:1118–1126. [PubMed: 19617884]
12. Dib-Hajj SD, Cummins TR, Black JA, Waxman SG. Sodium channels in normal and pathological pain. Annu Rev Neurosci. 2010; 33:325–347. [PubMed: 20367448]
13. Dib-Hajj SD, Tyrrell L, Black JA, Waxman SG. NaN, a novel voltage-gated Na channel, is expressed preferentially in peripheral sensory neurons and down-regulated after axotomy. Proc Natl Acad Sci U S A. 1998; 95:8963–8968. [PubMed: 9671787]
14. Dib-Hajj SD, Tyrrell L, Cummins TR, Black JA, Wood PM, Waxman SG. Two tetrodotoxin-resistant sodium channels in human dorsal root ganglion neurons. FEBS Lett. 1999; 462:117–120. [PubMed: 10580103]
15. Djouhri L, Fang X, Okuse K, Wood JN, Berry CM, Lawson SN. The TTX-resistant sodium channel Nav1.8 (SNS/PN3): expression and correlation with membrane properties in rat nociceptive primary afferent neurons. J Physiol. 2003; 550:739–752. [PubMed: 12794175]
16. Dover K, Solinas S, D'Angelo E, Goldfarb M. Long-term inactivation particle for voltage-gated sodium channels. J Physiol. 2010; 588:3695–3711. [PubMed: 20679355]
17. Fjell J, Cummins TR, Dib-Hajj SD, Fried K, Black JA, Waxman SG. Differential role of GDNF and NGF in the maintenance of two TTX-resistant sodium channels in adult DRG neurons. Brain Res Mol Brain Res. 1999; 67:267–282. [PubMed: 10216225]
18. Goetz R, Dover K, Laezza F, Shtraizent N, Huang X, Tchetchik D, Eliseenkova AV, Xu CF, Neubert TA, Ornitz DM, Goldfarb M, Mohammadi M. Crystal structure of a fibroblast growth factor homologous factor (FHF) defines a conserved surface on FHFs for binding and modulation of voltage-gated sodium channels. J Biol Chem. 2009; 284:17883–17896. [PubMed: 19406745]
19. Goldfarb M. Fibroblast growth factor homologous factors: evolution, structure, and function. Cytokine Growth Factor Rev. 2005; 16:215–220. [PubMed: 15863036]
20. Goldfarb M. Voltage-gated sodium channel-associated proteins and alternative mechanisms of inactivation and block. Cell Mol Life Sci. 2012; 69:1067–1076. [PubMed: 21947499]
21. Grieco TM, Malhotra JD, Chen C, Isom LL, Raman IM. Open-channel block by the cytoplasmic tail of sodium channel beta4 as a mechanism for resurgent sodium current. Neuron. 2005; 45:233–244. [PubMed: 15664175]
22. Grieco TM, Raman IM. Production of resurgent current in NaV1.6-null Purkinje neurons by slowing sodium channel inactivation with beta-pompilidotoxin. J Neurosci. 2004; 24:35–42. [PubMed: 14715935]
23. Hammer P, Banck MS, Amberg R, Wang C, Petznick G, Luo S, Khrebtukova I, Schroth GP, Beyerlein P, Beutler AS. mRNA-seq with agnostic splice site discovery for nervous system transcriptomics tested in chronic pain. Genome Res. 2010; 20:847–860. [PubMed: 20452967]
24. Herzog RI, Cummins TR, Ghassemi F, Dib-Hajj SD, Waxman SG. Distinct repriming and closed-state inactivation kinetics of Nav1.6 and Nav1.7 sodium channels in mouse spinal sensory neurons. J Physiol. 2003; 551:741–750. [PubMed: 12843211]
25. Ho C, O'Leary ME. Single-cell analysis of sodium channel expression in dorsal root ganglion neurons. Molecular and cellular neurosciences. 2011; 46:159–166. [PubMed: 20816971]

26. Hodgkin AL, Huxley AF. Currents carried by sodium and potassium ions through the membrane of the giant axon of Loligo. J Physiol. 1952; 116:449–472. [PubMed: 14946713]
27. Hubert T, Bourane S, Venteo S, Mechaly I, Puech S, Valmier J, Carroll P, Fichard-Carroll A. Fibroblast growth factor homologous factor 1 (FHF1) is expressed in a subpopulation of calcitonin gene-related peptide-positive nociceptive neurons in the murine dorsal root ganglia. J Comp Neurol. 2008; 507:1588–1601. [PubMed: 18220257]
28. Jarecki BW, Piekarz AD, Jackson JO 2nd, Cummins TR. Human voltage-gated sodium channel mutations that cause inherited neuronal and muscle channelopathies increase resurgent sodium currents. J Clin Invest. 2010; 120:369–378. [PubMed: 20038812]
29. Klinger AB, Eberhardt M, Link AS, Namer B, Kutsche LK, Schuy ET, Sittl R, Hoffmann T, Alzheimer C, Huth T, Carr RW, Lampert A. Sea-anemone toxin ATX-II elicits A-fiber-dependent pain and enhances resurgent and persistent sodium currents in large sensory neurons. Mol Pain. 2012; 8:69. [PubMed: 22978421]
30. Konig HG, Fenner BJ, Byrne JC, Schwamborn RF, Bernas T, Jefferies CA, Prehn JH. Fibroblast growth factor homologous factor 1 interacts with NEMO to regulate NF-kappaB signaling in neurons. J Cell Sci. 2012; 125:6058–6070. [PubMed: 23097049]
31. Koopmann TT, Bezzina CR, Wilde AA. Voltage-gated sodium channels: action players with many faces. Ann Med. 2006; 38:472–482. [PubMed: 17101538]
32. Leffler A, Herzog RI, Dib-Hajj SD, Waxman SG, Cummins TR. Pharmacological properties of neuronal TTX-resistant sodium channels and the role of a critical serine pore residue. Pflugers Arch. 2005; 451:454–463. [PubMed: 15981012]
33. Lewis AH, Raman IM. Cross-species conservation of open-channel block by Na channel beta4 peptides reveals structural features required for resurgent Na current. J Neurosci. 2011; 31:11527–11536. [PubMed: 21832183]
34. Lewis AH, Raman IM. Interactions among DIV voltage-sensor movement, fast inactivation, and resurgent Na current induced by the NaVbeta4 open-channel blocking peptide. J Gen Physiol. 2013; 142:191–206. [PubMed: 23940261]
35. Li GD, Wo Y, Zhong MF, Zhang FX, Bao L, Lu YJ, Huang YD, Xiao HS, Zhang X. Expression of fibroblast growth factors in rat dorsal root ganglion neurons and regulation after peripheral nerve injury. Neuroreport. 2002; 13:1903–1907. [PubMed: 12395088]
36. Liu C, Dib-Hajj SD, Waxman SG. Fibroblast growth factor homologous factor 1B binds to the C terminus of the tetrodotoxin-resistant sodium channel rNav1.9a (NaN). J Biol Chem. 2001; 276:18925–18933. [PubMed: 11376006]
37. Mikami M, Yang J. Short hairpin RNA-mediated selective knockdown of NaV1.8 tetrodotoxin-resistant voltage-gated sodium channel in dorsal root ganglion neurons. Anesthesiology. 2005; 103:828–836. [PubMed: 16192776]
38. Minett MS, Falk S, Santana-Varela S, Bogdanov YD, Nassar MA, Heegaard AM, Wood JN. Pain without nociceptors? Nav1.7-independent pain mechanisms. Cell Rep. 2014; 6:301–312. [PubMed: 24440715]
39. Miyazaki H, Oyama F, Inoue R, Aosaki T, Abe T, Kiyonari H, Kino Y, Kurosawa M, Shimizu J, Ogiwara I, Yamakawa K, Koshimizu Y, Fujiyama F, Kaneko T, Shimizu H, Nagatomo K, Yamada K, Shimogori T, Hattori N, Miura M, Nukina N. Singular localization of sodium channel beta4 subunit in unmyelinated fibres and its role in the striatum. Nat Commun. 2014; 5:5525. [PubMed: 25413837]
40. Munoz-Sanjuan I, Smallwood PM, Nathans J. Isoform diversity among fibroblast growth factor homologous factors is generated by alternative promoter usage and differential splicing. J Biol Chem. 2000; 275:2589–2597. [PubMed: 10644718]
41. Noda M, Shimizu S, Tanabe T, Takai T, Kayano T, Ikeda T, Takahashi H, Nakayama H, Kanaoka Y, Minamino N, et al. Primary structure of Electrophorus electricus sodium channel deduced from cDNA sequence. Nature. 1984; 312:121–127. [PubMed: 6209577]
42. Olsen SK, Garbi M, Zampieri N, Eliseenkova AV, Ornitz DM, Goldfarb M, Mohammadi M. Fibroblast growth factor (FGF) homologous factors share structural but not functional homology with FGFs. J Biol Chem. 2003; 278:34226–34236. [PubMed: 12815063]

43. Pablo JL, Pitt GS. Fibroblast Growth Factor Homologous Factors: New Roles in Neuronal Health and Disease. Neuroscientist. 2016; 22:19–25. [PubMed: 25492945]
44. Patel RR, Barbosa C, Xiao Y, Cummins TR. Human Nav1.6 Channels Generate Larger Resurgent Currents than Human Nav1.1 Channels, but the Navbeta4 Peptide Does Not Protect Either Isoform from Use-Dependent Reduction. PLoS One. 2015; 10:e0133485. [PubMed: 26182346]
45. Petryszak R, Burdett T, Fiorelli B, Fonseca NA, Gonzalez-Porta M, Hastings E, Huber W, Jupp S, Keays M, Kryvych N, McMurry J, Marioni JC, Malone J, Megy K, Rustici G, Tang AY, Taubert J, Williams E, Mannion O, Parkinson HE, Brazma A. Expression Atlas update–a database of gene and transcript expression from microarray- and sequencing-based functional genomics experiments. Nucleic Acids Res. 2014; 42:D926–932. [PubMed: 24304889]
46. Raman IM, Bean BP. Inactivation and recovery of sodium currents in cerebellar Purkinje neurons: evidence for two mechanisms. Biophys J. 2001; 80:729–737. [PubMed: 11159440]
47. Raman IM, Bean BP. Resurgent sodium current and action potential formation in dissociated cerebellar Purkinje neurons. J Neurosci. 1997; 17:4517–4526. [PubMed: 9169512]
48. Rush AM, Wittmack EK, Tyrrell L, Black JA, Dib-Hajj SD, Waxman SG. Differential modulation of sodium channel Na(v)1.6 by two members of the fibroblast growth factor homologous factor 2 subfamily. Eur J Neurosci. 2006; 23:2551–2562. [PubMed: 16817858]
49. Schaible HG. Peripheral and central mechanisms of pain generation. Handb Exp Pharmacol. 2007:3–28.
50. Schoorlemmer J, Goldfarb M. Fibroblast growth factor homologous factors and the islet brain-2 scaffold protein regulate activation of a stress-activated protein kinase. J Biol Chem. 2002; 277:49111–49119. [PubMed: 12244047]
51. Schoorlemmer J, Goldfarb M. Fibroblast growth factor homologous factors are intracellular signaling proteins. Curr Biol. 2001; 11:793–797. [PubMed: 11378392]
52. Sheets PL, Heers C, Stoehr T, Cummins TR. Differential block of sensory neuronal voltage-gated sodium channels by lacosamide [(2R)-2-(acetylamino)-N-benzyl-3-methoxypropanamide], lidocaine, and carbamazepine. J Pharmacol Exp Ther. 2008; 326:89–99. [PubMed: 18378801]
53. Sittl R, Lampert A, Huth T, Schuy ET, Link AS, Fleckenstein J, Alzheimer C, Grafe P, Carr RW. Anticancer drug oxaliplatin induces acute cooling-aggravated neuropathy via sodium channel subtype Na(V)1.6-resurgent and persistent current. Proc Natl Acad Sci U S A. 2012; 109:6704–6709. [PubMed: 22493249]
54. Smallwood PM, Munoz-Sanjuan I, Tong P, Macke JP, Hendry SH, Gilbert DJ, Copeland NG, Jenkins NA, Nathans J. Fibroblast growth factor (FGF) homologous factors: new members of the FGF family implicated in nervous system development. Proc Natl Acad Sci U S A. 1996; 93:9850–9857. [PubMed: 8790420]
55. Tan ZY, Piekarz AD, Priest BT, Knopp KL, Krajewski JL, McDermott JS, Nisenbaum ES, Cummins TR. Tetrodotoxin-resistant sodium channels in sensory neurons generate slow resurgent currents that are enhanced by inflammatory mediators. J Neurosci. 2014; 34:7190–7197. [PubMed: 24849353]
56. Theile JW, Jarecki BW, Piekarz AD, Cummins TR. Nav1.7 mutations associated with paroxysmal extreme pain disorder, but not erythromelalgia, enhance Navbeta4 peptide-mediated resurgent sodium currents. J Physiol. 2011; 589:597–608. [PubMed: 21115638]
57. Venkatesan K, Liu Y, Goldfarb M. Fast-Onset Long-Term Open-State Block of Sodium Channels by A-type FHFs Mediates Classical Spike Accommodation in Hippocampal Pyramidal Neurons. J Neurosci. 2014; 34:16126–16139. [PubMed: 25429153]
58. Wang C, Chung BC, Yan H, Lee SY, Pitt GS. Crystal structure of the ternary complex of a NaV C-terminal domain, a fibroblast growth factor homologous factor, and calmodulin. Structure. 2012; 20:1167–1176. [PubMed: 22705208]
59. Wang C, Hennessey JA, Kirkton RD, Wang C, Graham V, Puranam RS, Rosenberg PB, Bursac N, Pitt GS. Fibroblast growth factor homologous factor 13 regulates Na+ channels and conduction velocity in murine hearts. Circ Res. 2011; 109:775–782. [PubMed: 21817159]
60. Wang C, Wang C, Hoch EG, Pitt GS. Identification of novel interaction sites that determine specificity between fibroblast growth factor homologous factors and voltage-gated sodium channels. J Biol Chem. 2011; 286:24253–24263. [PubMed: 21566136]

61. Waxman SG, Cummins TR, Dib-Hajj S, Fjell J, Black JA. Sodium channels, excitability of primary sensory neurons, and the molecular basis of pain. Muscle Nerve. 1999; 22:1177–1187. [PubMed: 10454712]
62. Wildburger NC, Ali SR, Hsu WC, Shavkunov AS, Nenov MN, Lichti CF, LeDuc RD, Mostovenko E, Panova-Elektronova NI, Emmett MR, Nilsson CL, Laezza F. Quantitative proteomics reveals protein-protein interactions with fibroblast growth factor 12 as a component of the voltage-gated sodium channel 1.2 (nav1.2) macromolecular complex in Mammalian brain. Mol Cell Proteomics. 2015; 14:1288–1300. [PubMed: 25724910]
63. Wittmack EK, Rush AM, Craner MJ, Goldfarb M, Waxman SG, Dib-Hajj SD. Fibroblast growth factor homologous factor 2B: association with Nav1.6 and selective colocalization at nodes of Ranvier of dorsal root axons. J Neurosci. 2004; 24:6765–6775. [PubMed: 15282281]
64. Wu QF, Yang L, Li S, Wang Q, Yuan XB, Gao X, Bao L, Zhang X. Fibroblast growth factor 13 is a microtubule-stabilizing protein regulating neuronal polarization and migration. Cell. 2012; 149:1549–1564. [PubMed: 22726441]
65. Xiao HS, Huang QH, Zhang FX, Bao L, Lu YJ, Guo C, Yang L, Huang WJ, Fu G, Xu SH, Cheng XP, Yan Q, Zhu ZD, Zhang X, Chen Z, Han ZG, Zhang X. Identification of gene expression profile of dorsal root ganglion in the rat peripheral axotomy model of neuropathic pain. Proc Natl Acad Sci U S A. 2002; 99:8360–8365. [PubMed: 12060780]
66. Xie W, Strong JA, Kim D, Shahrestani S, Zhang JM. Bursting activity in myelinated sensory neurons plays a key role in pain behavior induced by localized inflammation of the rat sensory ganglion. Neuroscience. 2012; 206:212–223. [PubMed: 22265726]
67. Xie W, Strong JA, Li H, Zhang JM. Sympathetic sprouting near sensory neurons after nerve injury occurs preferentially on spontaneously active cells and is reduced by early nerve block. J Neurophysiol. 2007; 97:492–502. [PubMed: 17065247]
68. Xie W, Strong JA, Ye L, Mao JX, Zhang JM. Knockdown of sodium channel NaV1.6 blocks mechanical pain and abnormal bursting activity of afferent neurons in inflamed sensory ganglia. Pain. 2013; 154:1170–1180. [PubMed: 23622763]
69. Xie W, Strong JA, Zhang JM. Increased excitability and spontaneous activity of rat sensory neurons following in vitro stimulation of sympathetic fiber sprouts in the isolated dorsal root ganglion. Pain. 2010; 151:447–459. [PubMed: 20800969]
70. Xie W, Strong JA, Zhang JM. Local knockdown of the Na1.6 sodium channel reduces pain behaviors, sensory neuron excitability, and sympathetic sprouting in rat models of neuropathic pain. Neuroscience. 2015
71. Xie W, Tan ZY, Barbosa C, Strong JA, Cummins TR, Zhang JM. Upregulation of the sodium channel NaVbeta4 subunit and its contributions to mechanical hypersensitivity and neuronal hyperexcitability in a rat model of radicular pain induced by local DRG inflammation. Pain. 2015
72. Xie WR, Deng H, Li H, Bowen TL, Strong JA, Zhang J-M. Robust increase of cutaneous sensitivity, cytokine production and sympathetic sprouting in rats with localized inflammatory irritation of the spinal ganglia. Neuroscience. 2006; 142:809–822. [PubMed: 16887276]
73. Xie WR, Deng H, Li H, Bowen TL, Strong JA, Zhang JM. Robust increase of cutaneous sensitivity, cytokine production and sympathetic sprouting in rats with localized inflammatory irritation of the spinal ganglia. Neuroscience. 2006; 142:809–822. [PubMed: 16887276]
74. Yan H, Pablo JL, Pitt GS. FGF14 regulates presynaptic Ca2+ channels and synaptic transmission. Cell Rep. 2013; 4:66–75. [PubMed: 23831029]
75. Yan H, Pablo JL, Wang C, Pitt GS. FGF14 modulates resurgent sodium current in mouse cerebellar Purkinje neurons. Elife. 2014; 3:e04193. [PubMed: 25269146]
76. Zhang, JM. Localized Inflammatory Irritation of the Lumbar Ganglia: An Animal Model of Chemogenic Low Back Pain and Radiculopathy. In: Ma, C., Zhang, J-M., editors. Animal Models of Pain. Springer Protocols: Humana Press; 2011. p. 89-102.
77. Zhang X, Bao L, Yang L, Wu Q, Li S. Roles of intracellular fibroblast growth factors in neural development and functions. Sci China Life Sci. 2012; 55:1038–1044. [PubMed: 23233218]

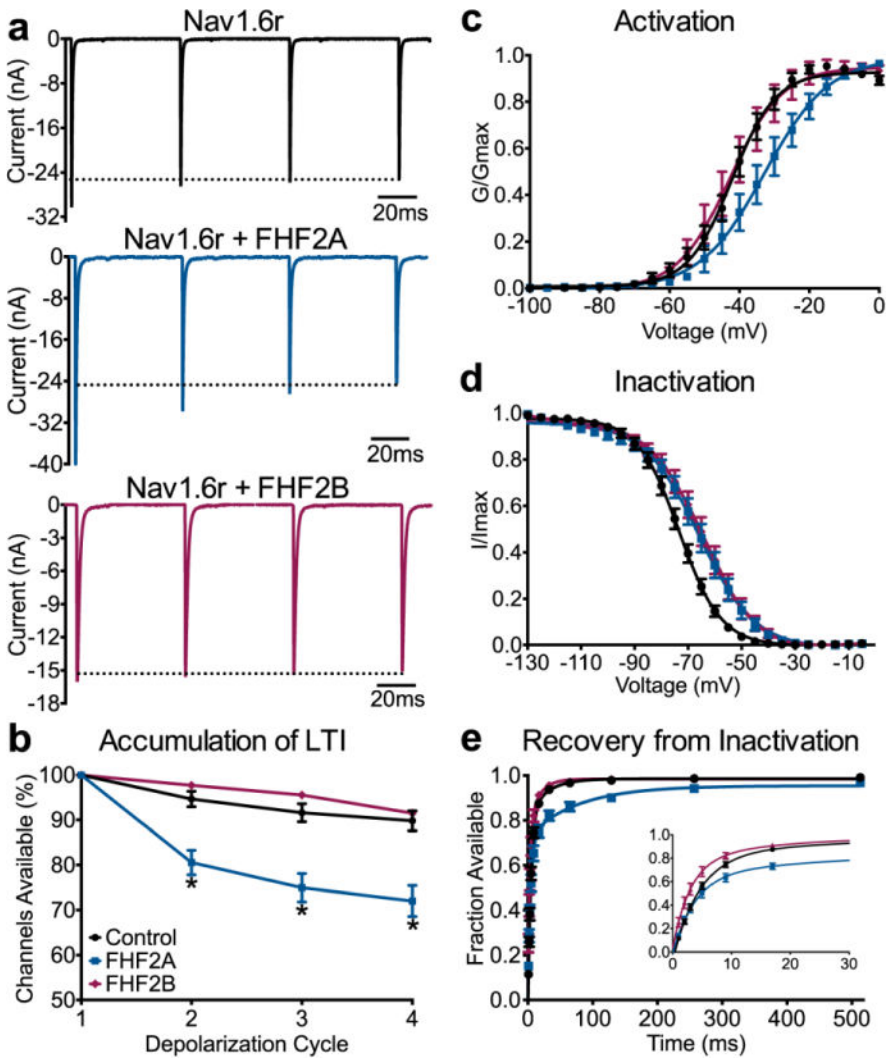

Fig. 1. Biophysical properties of Nav1.6r modulated by FHF2A and FHF2B

DRG neurons were transfected with Nav1.6r and FHF2A, FHF2B or fluorescent protein tag (control). ***a***, Representative traces of cycle-dependent reduction as a measure of accumulation of long-term inactivation (LTI) for control (black), FHF2A (blue) and FHF2B (purple) groups. ***b***, The percentage of channels available as a function of depolarization cycle shows overexpression of FHF2A (n=19) increased accumulation of long-term relative to control (n=28), whereas, FHF2B (n=13) did not. Activation, inactivation and recovery from inactivation were assayed with a series of standard protocols (see **Methods** sections). ***c***, Normalized conductance (G/Gmax) as a function of voltage shows that FHF2A (blue squares, n=16) overexpression shifted the voltage dependence of activation relative to control (black circles, n=25). No change is observed for FHF2B overexpression (purple diamonds, n=11) relative to control. ***d***, Normalized current (I/Imax) as a function of voltage shows that voltage dependence of inactivation was shifted to positive potentials in FHF2A (n=19) and FHF2B (n=13) groups relative to control (n=27). ***e***, Fraction of channels available as a function of time shows FHF2A (n=19) overexpression greatly slowed recovery from inactivation relative to control (n=15), whereas, FHF2B (Inset, n=12) enhanced

channel recovery. Abbreviations: LTI-Long-term Inactivation; Asterisks (*) represent $p < 0.0001$ obtained from Student's t-test. Data are mean ± SEM.

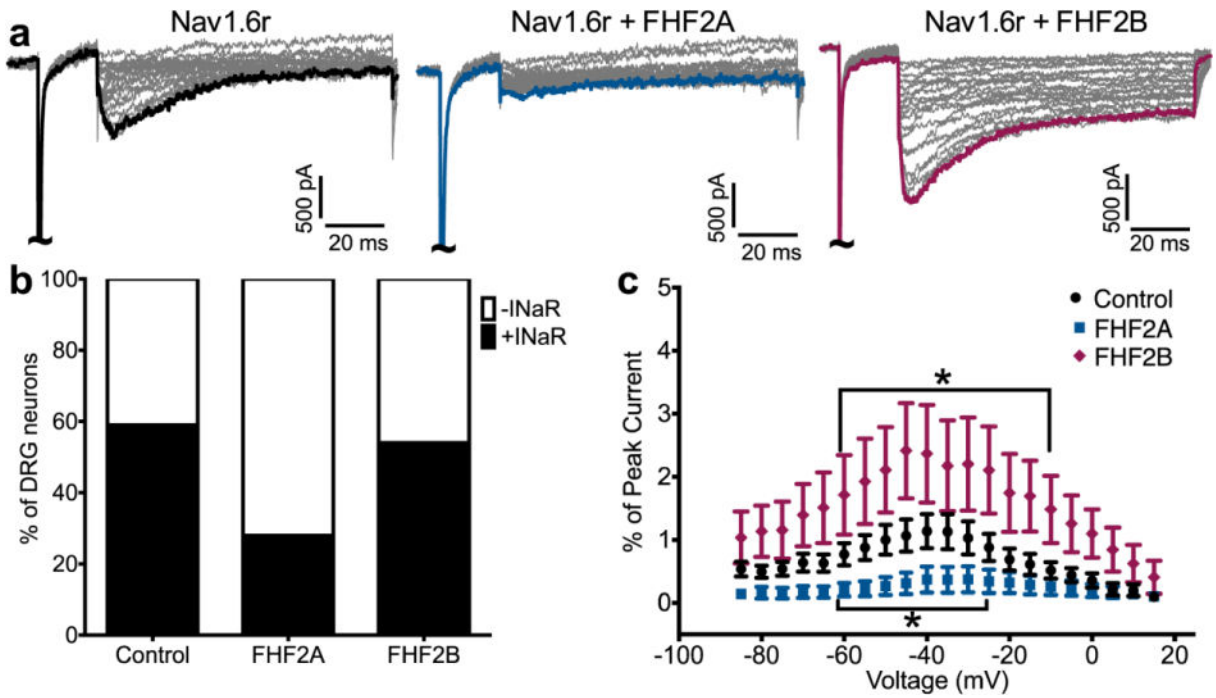

Fig. 2. FHF2A and FHF2B differentially regulate fast resurgent currents

a, Representative traces of Nav1.6r mediated resurgent currents obtained from cultured DRG neurons with corresponding peak resurgent currents highlighted for control (black), FHF2A overexpression (blue) and FHF2B overexpression (purple) conditions. ***b***, The distribution of resurgent current positive (+INaR)/resurgent current negative (−INaR) DRG neurons was not different with FHF2B (n=13) overexpression relative to control (n=29). FHF2A (n=18) overexpression significantly decreased the percentage of DRG neurons that generated resurgent currents relative to control ($p<0.0005$, X^2 test). ***c***, Normalized resurgent current amplitude as a function of voltage shows FHF2A overexpression (blue squares) decreased resurgent current amplitude in a range of voltages relative to control (black circles). In contrast, FHF2B overexpression (purple triangles) increased resurgent current amplitude in a range of voltages. Asterisks (*) represent $p < 0.05$ obtained from Student's t-test. Data are mean ± SEM.

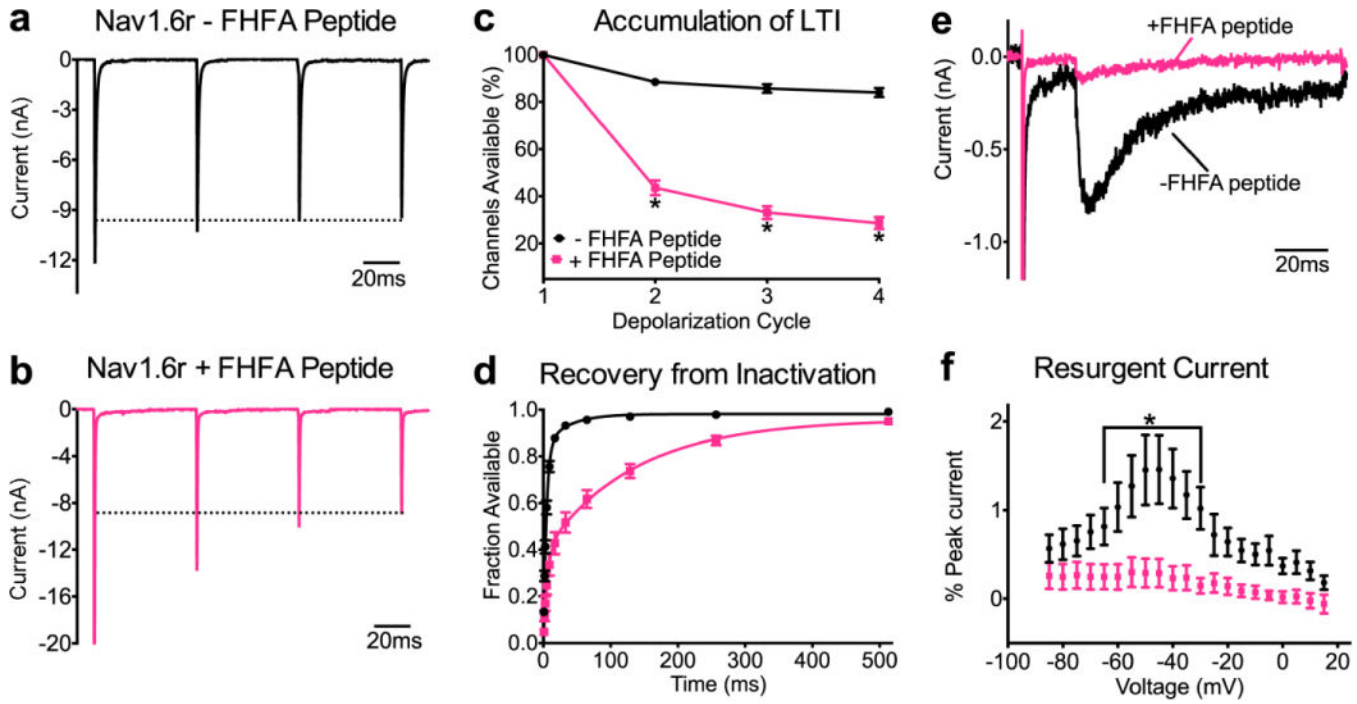

Fig. 3. FHFA peptide exhibits long-term inactivation activity and recapitulates resurgent current reduction effects

Nav1.6r currents were isolated in DRG neurons and recordings were obtained in the presence (+) or absence (−) of FHFA peptide in the recording pipette. Representative traces of cycle-dependent reduction as a measure of accumulation of long-term inactivation (LTI) are shown for −FHFA peptide group (***a***, black) and +FHFA peptide group (***b***, pink). ***c***, The percentage of channels available as a function of depolarization cycles shows that addition of the FHFA peptide (black circles, n=15) significantly increased accumulation of channels in long-term inactivated states relative to −FHFA peptide group (pink squares, n=14). ***d***, Recovery from inactivation was greatly slowed in +FHFA peptide group (n=15) relative to −FHFA peptide group (n=14). ***e***, Representative traces of Nav1.6r mediated resurgent currents with peak currents highlighted for −FHFA peptide (black) and +FHFA peptide (pink) groups. ***f***, Compared to −FHFA peptide (black circles, n=15), addition of the FHFA peptide (pink squares, n=16) reduced resurgent current amplitude. Note resurgent currents were normalized to peak transient currents and plotted as a function of voltage. Abbreviations: LTI-Long-term Inactivation. Asterisks (*) represent $p<0.05$ obtained from Student's t-test. Data are mean ± SEM.

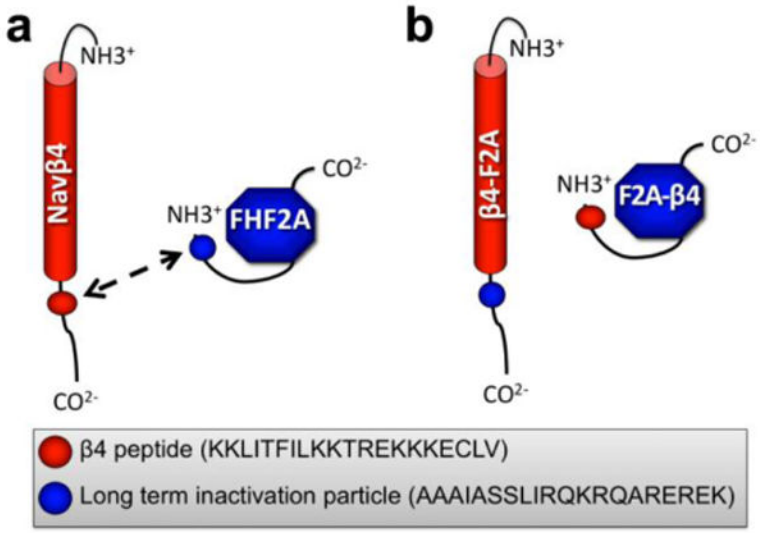

Fig. 4. Chimeric constructs of FHF2A and *Navβ4*

a, Illustration of FHF2A and Navβ4 subunits. The Navβ4 subunit consists of an extracellular N-terminal domain, a single transmembrane domain and a cytosolic C-terminal domain. The cytosolic domain contains a sequence of amino acids proposed to mediate open channel block that generate resurgent currents (red sphere represents β4 peptide sequence, amino acids 183–203(2, 33)). The FHF2A subunit is a cytosolic protein, which contains a core region homologous to all FHF with a C-terminal epitope that enables interaction with the cytoplasmic C-terminal region of sodium channels (18). Distinct from its FHF2B counterpart, the FHF2A N-terminus sequence is much longer and contains a sequence identified as the long-term inactivation particle (blue sphere, amino acids 1–20 (16)). Arrow between the subunit highlights the region that was exchanged between these subunits to generate the chimeric constructs. ***b***, Illustration of the resulting chimeric constructs. The (β4)F2A contains all components of the Navβ4 subunit with the exception of β4-peptide sequence, which was replaced with long-term inactivation particle sequence. The F2A(β4) contains all domains of the FHF2A protein except the long-term inactivation particle, which was replaced with the β4 peptide sequence. ***Inset***, depicts the figure legend for the β4-peptide and long-term inactivation particle with the corresponding amino acid sequence.

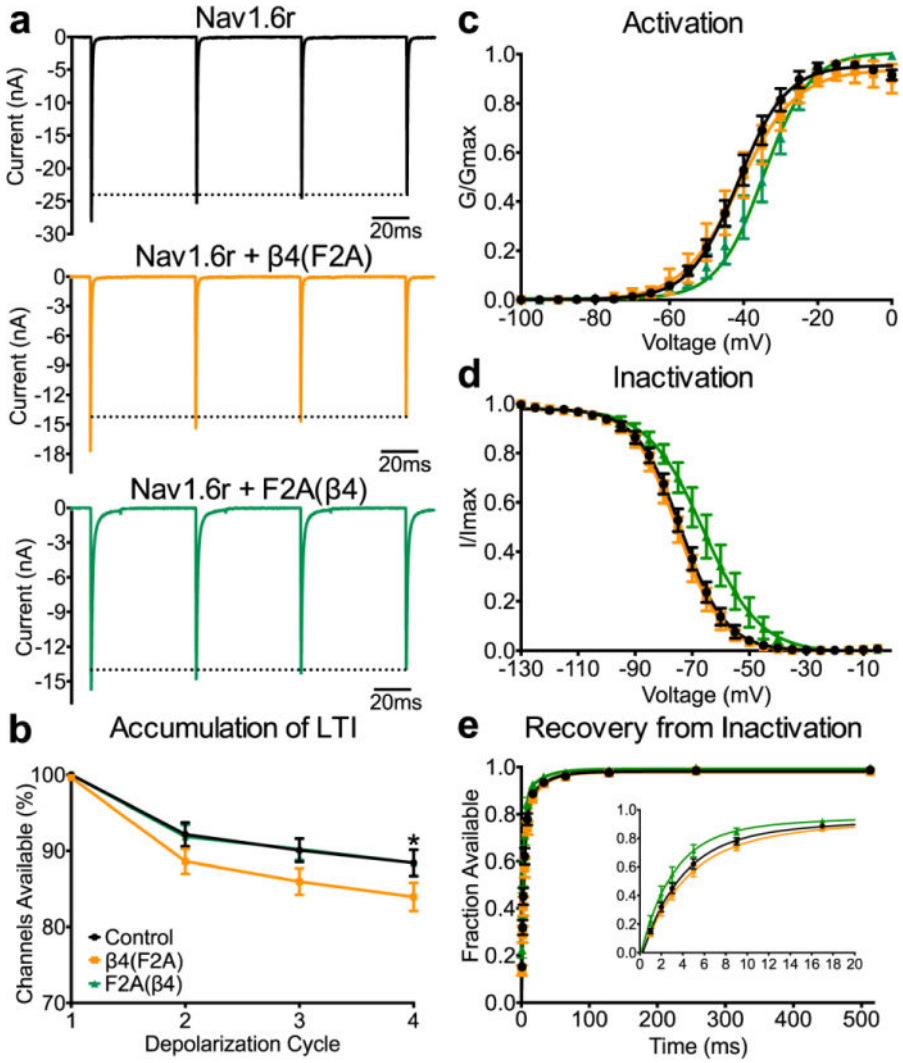

Fig. 5. Biophysical properties of Nav1.6r modulated by β4(F2A) and F2A(β4) chimeras

Activation, inactivation and recovery from inactivation were assayed with a series of standard protocols (see **Methods** sections). ***a***, Representative traces of cycle-dependent reduction as a measure of long-term inactivation (LTI) for Nav1.6r isolated currents in DRG neurons with co-expression of fluorescent tag (control, black), F2A(β4) (green) and β4-F2A (orange). ***b***, The percentage of channels available as a function of depolarization cycle shows increased accumulation of long-term inactivation for β4(F2A) group (orange squares, n=12) relative to control (black circles, n=16), whereas no difference is observed for F2A(β4) group (green triangles, n=8) relative to control. ***c***, Normalized conductance as a function of voltage shows that co-expression of F2A(β4) (n=8) shifted the voltage dependence of activation to positive potentials relative to control (n=14), whereas, no change is observed for the β4(F2A) group (n=12). ***d***, Normalized current as a function of voltage shows that co-expression of F2A(β4) (n=9) shifted the voltage dependence of steady-state inactivation to positive potentials relative to control (n=14), whereas, no change is observed for the β4(F2A) group (n=12). ***e***, Fraction of current available as a function of time shows that recovery is not significantly altered with co-expression of either chimera β4(F2A) (n=12) or

F2A(β4) (n=9) relative to control (n=14). Asterisks (*) represent $p<0.05$ obtained from Student's t-test. Data are mean ± SEM.

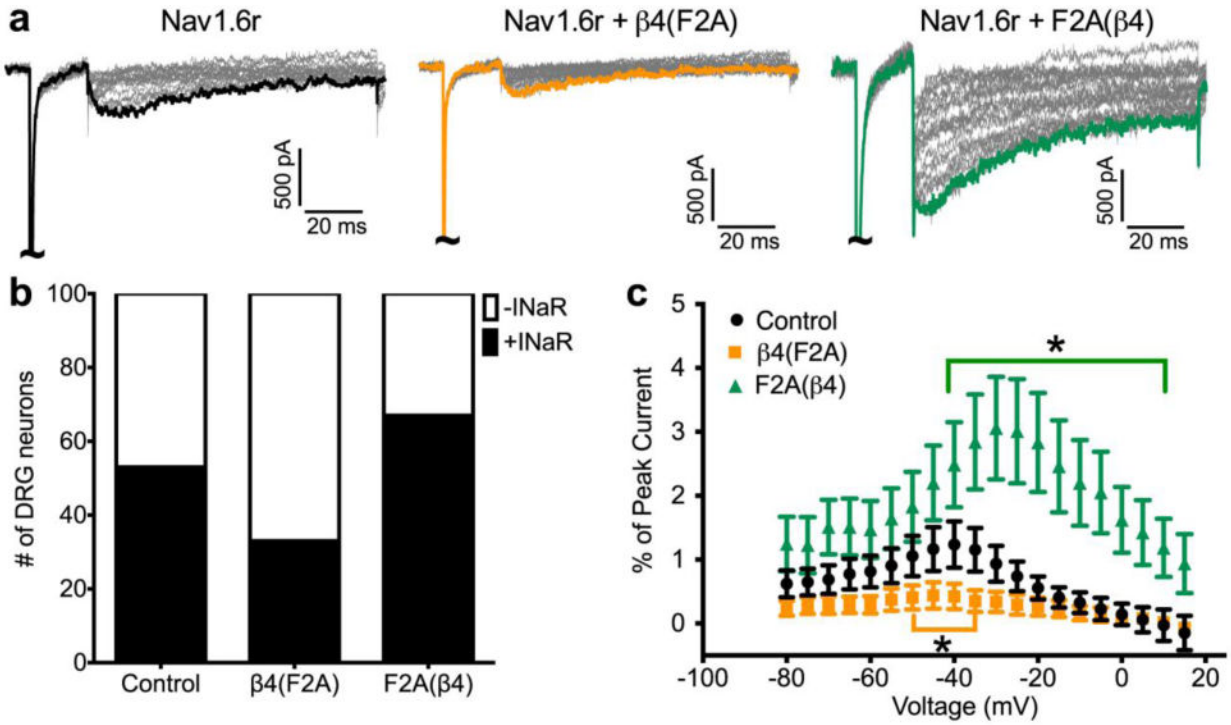

Fig. 6. *β4*(F2A) and F2A(*β4*) differentially modulate fast resurgent currents

a, Representative traces of Nav1.6r mediated resurgent currents obtained from cultured DRG neurons with corresponding peak resurgent currents highlighted for control (black), β4(F2A) (orange) and F2A(β4) (green) groups. ***b***, Neither co-expression of (β4)F2A (n=12) nor co-expression of F2A(β4) (n=9) altered the distribution of resurgent current positive (+INaR)/ resurgent current negative (−INaR) DRG neurons relative to control (n=16). ***c***, Resurgent current amplitude was decreased with co-expression of β4(F2A) (orange squares, n=12) in a range of voltages relative to control (black circles, n=15). In contrast, co-expression of F2A(β4) (green triangles, n=9) chimera increased resurgent current amplitude in a range of voltages relative to control. Note that resurgent currents were normalized to peak transient currents and plotted as a function of voltage. Asterisks (*) represent $p < 0.05$ obtained from Student's t-test. Summary data are mean ± SEM.

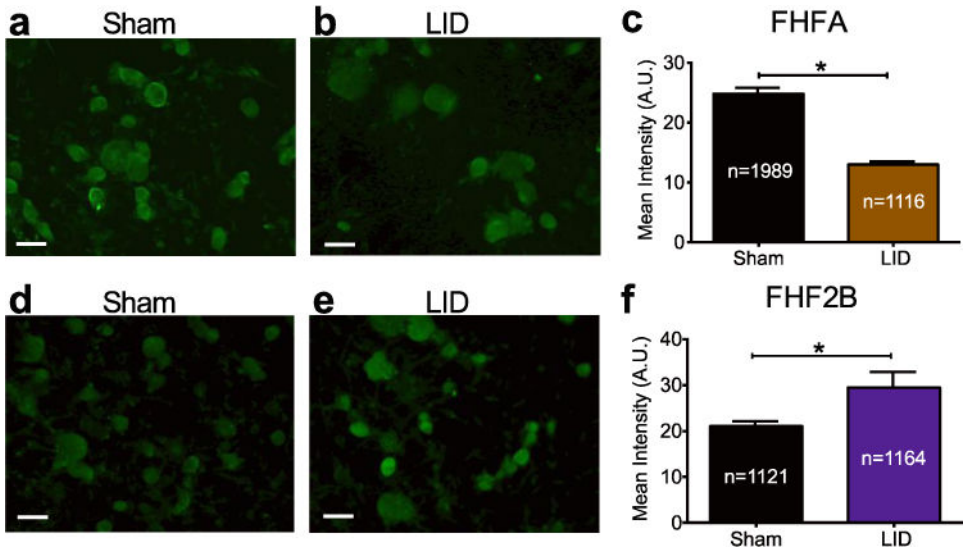

Fig. 7. FHFA and FHF2B levels are differentially altered after local inflammation of the DRG

Examples of immunocytochemical staining for FHFAs in primary cultured DRG neurons from control (sham operated, ***a***) and induced local inflammation of the DRGs (LID, ***b***) animals post-operative day 5. ***c***, DRG neurons from LID animals (n=1989) exhibited an increase in FHFA signal relative to sham control (n=1116). Examples of immunocytochemical staining for FHF2B in primary cultured DRG neurons from control (sham operated, ***d***) and induced local inflammation of the DRGs (LID, ***e***) animals post-operative day 5. ***f***, DRG neurons from LID animals (n=1164) exhibited a decrease in FHF2B signal relative to sham control (n=1121). Five animals per group were examined. Asterisks (*) represent $p < 0.0001$ obtained from Student's t-test. Summary data are mean ± SEM. Scale bar 50 μm.

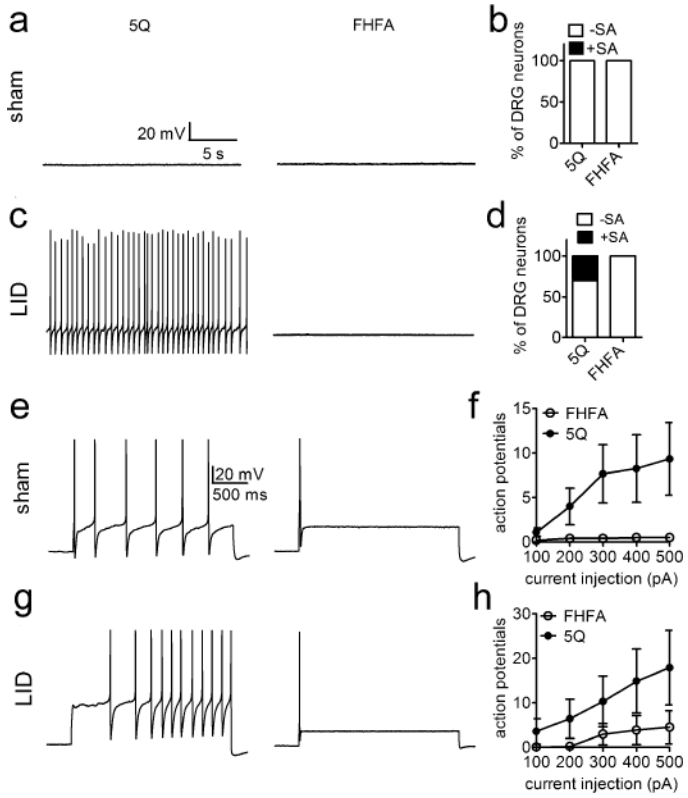

Fig. 8. FHFA peptide reduces excitability of DRG neurons

a-b, No spontaneous activity (-SA) was detected on DRG neurons from sham rats when 1 mM FHFA (n = 10) or 1 mM 5Q (n = 12) was included in the pipette solution. **c-d**, 30% of DRG neurons from local inflammation of the DRGs (LID) rats showed spontaneous activity (+SA) in the presence of 1 mM 5Q (n = 10), while no spontaneous activity was observed in the presence of 1 mM FHFA (n = 14). Representative action potential traces induced by a 2-s injection of 400 pA current on DRG neurons from sham (**e**) and LID (**f**) rats in the presence of 1 mM 5Q (left panel) or 1 mM FHFA (right panel). **f and h**, average number of action potentials induced by 2-s injection of currents ranging from 100 – 500 pA.

Table 1

FHF2A/B: Biophysical Properties of Nav1.6r in control, FHF2A and FHF2A groups

	Current Density (nA/pF)	Activation		Inactivation		Recovery	
		$V_{1/2}$ (mV)	k	$V_{1/2}$ (mV)	k	τfast (ms)	τslow (ms)
Control	2.0 ± 0.2	−41.0 ± 1.9	4.4 ± 0.4	−73.5 ± 1.4	6.7 ± 0.2	5.1 ± 0.5	29.0 ± 3.8
n	25	25	25	27	27	15	15
FHF2A	2.9 ± 0.5	−32.5 ± 2.7*	5.2 ± 0.5	−65.6 ± 2.0*	8.0 ± 0.5	4.9 ± 0.8	141.1 ± 41†
n	16	16	16	19	19	19	19
FHF2B	1.6 ± 0.3	−41.0 ± 3.4	4.9 ± 0.5	−64.8 ± 2.5*	8.1 ± 0.6	3.2 ± 0.6*	17.7 ± 4.4
n	11	11	11	13	13	12	12

Abbreviations are: τ, time constant; k, slope factor of activation or inactivation curve; $V_{1/2}$, midpoint of activation or inactivation curve. Groups were compared to control using Student's t-test (parametric) or Mann-Whitney U Test (non-parametric).

*p<0.05 (*vs* control);

#p<0.005 (*vs* control);

†p<0.0001 (*vs* control). Data are mean ± SEM

Table 2

Biophysical Properties of Nav1.6r with or without FHFA peptide

	Current Density (nA/pF)	Activation		Inactivation		Recovery	
		$V_{1/2}$ (mV)	k	$V_{1/2}$ (mV)	k	τfast (ms)	τslow (ms)
−FHFA	1.7 ± 0.4	−39.0 ± 2.6	5.8 ± 0.6	−71.2 ± 1.4	6.3 ± 0.3	5.1 ± 0.6	35.4 ± 7.8 *
n	16	16	16	16	16	16	16
+FHFA	0.9 ± 0.1	−38.5 ± 2.6	6.5 ± 0.3	−75.1 ± 2.2	5.7 ± 0.3	7.0 ± 0.8	139.5 ± 11 †
n	14	14	14	15	15	15	15

Abbreviations are: τ, time constant; k, slope factor of activation or inactivation curve; $V_{1/2}$, midpoint of activation or inactivation curve. Groups were compared using Mann-Whitney t-test or Student's t-test.

* p<0.05;

† p<0.0001. Data are mean ± SEM

Table 3

Chimeric Experiment: Biophysical Properties of Nav1.6r in control, F2A(β4) and β4(F2A) groups

	Current Density (nA/pF)	Activation		Inactivation		Recovery	
		$V_{1/2}$ (mV)	k	$V_{1/2}$ (mV)	k	τfast (ms)	τslow (ms)
Control	4.2 ± 2.6	−40.3 ± 1.7	6.1 ± 0.8	− 73.8 ± 1.6	7.3 ± 0.3	4.8 ± 0.5	38.8 ± 5.6
n	14	14	14	14	14	14	14
β4(F2A)	1.6 ± 0.3	−40.5 ± 3.2	5.2 ± 0.5	−75.17 ± 1.8	7.2 ± 0.4	4.8 ± 0.7	35.6 ± 7.1
n	12	12	12	12	12	12	12
F2A(β4)	1.1 ± 0.3	−35.2 ± 2.5*	6.0 ± 0.5	−65.3 ± 3.3*	7.4 ± 0.4	2.7 ± 0.3*	43.0 ± 11
n	9	8	8	9	9	9	9

Abbreviations are: τ, time constant; k, slope factor of activation or inactivation curve; $V_{1/2}$, midpoint of activation or inactivation curve. Groups were compared to control using Student's t-test (parametric) or Mann-Whitney U Test (nonparametric).

*p<0.05 (*vs* control). Data are mean ± SEM